

1 **Heterogeneous chemistry: a mechanism missing in**
2 **current models to explain secondary inorganic**
3 **aerosol formation during the January 2013 haze**
4 **episode in North China**

5 **B. Zheng¹, Q. Zhang^{2,5}, Y. Zhang^{3,1,5}, K. B. He^{1,4,5}, K. Wang³, G. J. Zheng¹,**
6 **F. K. Duan¹, Y. L. Ma¹, and T. Kimoto⁶**

7

8 [1] {State Key Joint Laboratory of Environment Simulation and Pollution Control,
9 School of Environment, Tsinghua University, Beijing, China}

10 [2] {Ministry of Education Key Laboratory for Earth System Modeling, Center for
11 Earth System Science, Tsinghua University, Beijing, China}

12 [3] {Department of Marine, Earth and Atmospheric Sciences, North Carolina State
13 University, Raleigh, North Carolina, USA}

14 [4] {State Environmental Protection Key Laboratory of Sources and Control of Air
15 Pollution Complex, Beijing 100084, China}

16 [5] {Collaborative Innovation Center for Regional Environmental Quality, Beijing
17 100084, China}

18 [6] {Kimoto Electric Co., Ltd, 3-1 Funahashi-cho Tennoji-ku Osaka, 543-0024 Japan}

19

20

21

22

23

24

25

26

27

28 Correspondence to: Q. Zhang (qiangzhang@tsinghua.edu.cn)

29 K. B. He (hekb@tsinghua.edu.cn)

Abstract

Severe regional haze pollution events occurred in eastern and central China in January 2013, which had adverse effects on the environment and public health. Extremely high levels of particulate matter with aerodynamic diameter of 2.5 μm or less ($\text{PM}_{2.5}$) with dominant components of sulfate and nitrate are responsible for the haze pollution. Although heterogeneous chemistry is thought to play an important role in the production of sulfate and nitrate during haze episodes, few studies have comprehensively evaluated the effect of heterogeneous chemistry on haze formation in China by using the 3D models due to of a lack of treatments for heterogeneous reactions in most climate and chemical transport models. In this work, the WRF-CMAQ model with newly added heterogeneous reactions is applied to East Asia to evaluate the impacts of heterogeneous chemistry and the meteorological anomaly during January 2013 on regional haze formation. As the parameterization of heterogeneous reactions on different types of particles is not well established yet, we arbitrarily selected the uptake coefficients from reactions on dust particles and then conducted several sensitivity runs to find the value that can best match observations. The revised CMAQ with heterogeneous chemistry not only captures the magnitude and temporal variation of sulfate and nitrate, but also reproduces the enhancement of relative contribution of sulfate and nitrate to $\text{PM}_{2.5}$ mass from clean days to polluted haze days. These results indicate the significant role of heterogeneous chemistry in regional haze formation and improve the understanding of the haze formation mechanisms during the January 2013 episode.

54 **1. Introduction**

55 Regional haze pollution is an atmospheric phenomenon characterized by
56 significant growth in the concentration of aerosol particles and sharp reduction of
57 visibility. In addition to the adverse effects on visibility, haze pollution also affects the
58 air quality, public health, and climate. By scattering and absorbing solar radiation,
59 aerosol particles suspended within haze can decrease the fluxes of solar radiation
60 reaching the earth's surface, significantly altering the earth's energy budget and
61 climate (Seinfeld et al., 2004; Mercado et al., 2009). Sulfate and nitrate aerosols can
62 increase soil acidity through acid deposition, which has a negative impact on the
63 ecosystem (Zhao et al., 2009). Because of their small sizes, aerosol particles can
64 penetrate deeply into human lungs, causing respiratory diseases, decreased lung
65 function, and increased risk of cancer and mortality (American Lung Association,
66 2006).

67 Haze pollution in China is of significant concern because of its increased
68 frequency of occurrence in recent years. The number of haze days has shown an
69 increasing trend since the 1990s and visibility during the haze events has decreased
70 rapidly (Zhao et al., 2011; Ding and Liu, 2014). Aerosol loadings during haze days
71 can be extremely high with maximum hourly concentrations of particulate matter with
72 aerodynamic diameter of 2.5 μm or less ($\text{PM}_{2.5}$) of 200–1000 $\mu\text{g m}^{-3}$ (Sun et al., 2006;
73 Wang et al., 2006; X. J. Zhao et al., 2013; L. T. Wang et al., 2014; Y. S. Wang et al.,
74 2014), which can reduce surface solar radiation by more than 20 W m^{-2} (Li et al.,
75 2007).

76 Most parts of central and eastern China experienced a persistent episode of haze
77 pollution during January 2013, which is one of the most severe air pollution episodes
78 in China during the last decade (He et al., 2014; Y. S. Wang et al., 2014; Z. F. Wang et
79 al., 2014; J. K. Zhang et al., 2014; R. H. Zhang et al., 2014). Widespread haze clouds
80 covered the entire North China Plain (NCP) (Yang et al., 2013) and the instantaneous
81 concentration of $\text{PM}_{2.5}$ within these clouds exceeded 1000 $\mu\text{g m}^{-3}$ at some urban
82 observational sites (Y. S. Wang et al., 2014). The characteristics and formation
83 mechanisms of this haze event attract considerable attention from the scientific
84 community.

85 High emission intensity, adverse meteorological conditions, and the formation of
86 substantial amounts of secondary aerosols are generally regarded as the principal
87 factors underlying the formation of the severe haze pollution in January 2013. Central

88 and eastern China are the most important source regions of anthropogenic emissions
89 in China (Zhang et al., 2009), which can provide sufficient precursors for haze
90 formation. Adverse meteorological conditions in January 2013 conducive to haze
91 formation include weak surface winds, low mixing layers, a thick temperature
92 inversion layer, and anomalous southerly winds in the middle and lower troposphere
93 that transport large amounts of water vapor and pollutants (Y. S. Wang et al., 2014; R.
94 H. Zhang et al., 2014). Under weather conditions of high humidity and reduced
95 advection and vertical mixing, large amounts of secondary aerosols (both organic and
96 inorganic) can be generated. In particular, greater amounts of secondary inorganic
97 aerosols comprising sulfate, nitrate, and ammonium (SNA) were produced during the
98 haze days of the January 2013 episode than during clean days. The contribution of
99 sulfate and nitrate to $PM_{2.5}$ increased from 10.3–13.4% and 6.6–14% in clean days to
100 25.1% and 17.5–20.6% in haze days, respectively (J. K. Zhang et al., 2014; Quan et
101 al., 2014). The total contribution of SNA reached about 60% during the most severe
102 haze days from 12–15 January (J. K. Zhang et al., 2014; Quan et al., 2014), which
103 indicates that the significant production of SNA is a principal driving force that leads
104 to the sharp increase in $PM_{2.5}$ concentrations.

105 Many studies on aerosols have revealed that SNA are the most abundant
106 component of $PM_{2.5}$ during haze pollution events in China, and that the processes and
107 evolution of haze pollution are characterized by the formation of substantial amounts
108 of sulfate and nitrate (Sun et al., 2006; Wang et al., 2006; X. J. Zhao et al., 2013). The
109 formation mechanisms are difficult to be explained by traditional gas-phase or
110 aqueous-phase chemistry (i.e., gas-phase oxidation by hydroxyl radical (OH) and in-
111 cloud oxidation by dissolved ozone (O_3) and hydrogen peroxide (H_2O_2)) given the
112 adverse atmospheric conditions (i.e. low or even zero O_3 concentrations, dim days
113 with low solar radiations and few precipitating clouds) (X.J. Zhao et al., 2013; Quan
114 et al., 2014). Besides the gas-phase and aqueous-phase chemistry, heterogeneous
115 chemistry is considered to be alternative pathways of sulfate and nitrate formation in
116 the atmosphere (Ravishankara, 1997). The ambient measurement has verified the
117 existence of heterogeneous reactions associated with sulfur dioxide (SO_2), nitrogen
118 pentoxide (N_2O_5) and nitric acid (HNO_3) (Usher et al., 2003; Lammel and Leip, 2005;
119 McNaughton et al., 2009; Chang et al., 2011). Field studies during haze days in China
120 proposed that the large amount of sulfate and nitrate were more likely generated via
121 heterogeneous chemistry than gas-phase and aqueous-phase chemistry (Wang et al.,

122 2006; Li and Shao, 2009, 2010; Li et al., 2011; X. Wang et al., 2012; X. J. Zhao et al.,
123 2013; Y. S. Wang et al., 2014). Modeling studies have used 0-3D air quality models to
124 research on the role of heterogeneous reactions in sulfate and nitrate formation on the
125 surface of mineral particles (Zhang et al., 1994; Dentener et al., 1996; Zhang and
126 Carmichael, 1999; K. Wang et al., 2012). However, few studies have comprehensively
127 evaluated the effect of heterogeneous chemistry on haze formation in China by using
128 the 3D models because of a lack of treatments for heterogeneous reactions in most
129 climate and chemical transport models.

130 In this work, we use the CMAQ model to investigate the impact of
131 heterogeneous chemistry on the severe regional haze formation in January 2013. The
132 officially-released version of CMAQ (hereafter the original CMAQ) and revised
133 CMAQ with updated treatments for heterogeneous chemistry by adding a number of
134 reactions (hereafter the revised CMAQ) are applied to simulate the January 2013
135 severe regional haze pollution episode over East Asia. Our objectives are to improve
136 the model's capability in reproducing the observed high PM concentrations and
137 provide better understanding of the effects of heterogeneous reactions on the
138 production of sulfate and nitrate during the haze event.

139

140 **2. Model Description and Methodology**

141 In this work, the Weather Research and Forecasting (WRF) model v3.5.1
142 (<http://www.wrf-model.org/>) and CMAQ v5.0.1 (<http://www.cmascenter.org/cmaq/>)
143 are applied to simulate the severe haze episode in January 2013 over East Asia. WRF
144 is a new generation mesoscale numerical weather prediction system designed to serve
145 a wide range of meteorological applications from meters to thousands of kilometers
146 (<http://www.wrf-model.org/>). WRF v3.5.1 is the most recent major WRF release in
147 September 2013 and is used to generate meteorological fields to drive CMAQ.
148 CMAQ is a 3D Eulerian atmospheric chemistry and transport modeling system that
149 simulates multi pollutants throughout the troposphere across spatial scales ranging
150 from local to hemispheric. CMAQ v5.0.1 is the most up to date release in July 2012.
151 It contains the updated carbon bond gas-phase mechanism with new toluene
152 chemistry (Whitten et al., 2010), a new aerosol module (AERO6), and ISORROPIA
153 v2.1 inorganic chemistry (Fountoukis and Nenes, 2007). The existing formation
154 mechanisms for SNA included in the original CMAQ and new heterogeneous
155 reactions added in the revised CMAQ that form additional SNA are described below.

156 2.1. The Formation Mechanisms of SNA in the Original CMAQ

157 Table 1 summarizes major mechanisms for sulfate and nitrate formation
158 currently treated in the original CMAQ v5.0.1 (R1–R15) in a highly simplified
159 manner. In the gas-phase (R1–R6), sulfuric acid (H_2SO_4) and HNO_3 are generated
160 mainly through the oxidation of SO_2 and nitrogen oxide (NO_x) by OH. Additional
161 HNO_3 can be formed through subsequent reactions involving reactive nitrogen species
162 such as nitrogen trioxide (NO_3), N_2O_5 , and NTR and OH, hydroperoxyl radical (HO_2),
163 and H_2O as well as the nighttime oxidation reaction of volatile organic compounds
164 (VOCs) by NO_3 . H_2SO_4 and HNO_3 can condense on the surface of preexisting
165 aerosol, forming sulfate (SO_4^{2-}) and nitrate (NO_3^-). For in-cloud chemistry (R7–R13),
166 the original CMAQ includes the dissolution equilibria of SO_2 , H_2SO_4 , ammonia
167 (NH_3), NO_x , NO_3 , N_2O_5 , nitrous acid (HNO_2), HNO_3 , peroxyntiric acid (HNO_4), and
168 several oxidants such as OH, H_2O_2 , and O_3 , the dissociation equilibria of SO_2 ,
169 bisulfite (HSO_3^-), HNO_2 , HNO_3 , and $\text{NH}_3 \cdot \text{H}_2\text{O}$, and five aqueous-phase kinetic
170 reactions to produce S (VI) through the oxidation of S (IV) (dissolved SO_2 , HSO_3^-
171 and sulfite (SO_3^{2-})) by H_2O_2 , methylhydroperoxide (MHP), peroxyacetic acid (PAA),
172 O_3 , and oxygen (O_2) catalyzed by ferric iron (Fe^{3+}) and manganese ion (Mn^{2+}). Once
173 clouds dissipate, SO_4^{2-} formed in the aqueous-phase becomes part of aerosol. The
174 original CMAQ only includes two heterogeneous reactions (R14–R15) to produce
175 HNO_3 , one involving N_2O_5 and H_2O and the other involving nitrogen dioxide (NO_2)
176 and H_2O . The mechanism of heterogeneous chemistry is much more complex than the
177 homogeneous gas and aqueous-phase mechanisms. It involves many processes
178 including water condensation onto the particle surfaces, adsorption and
179 accommodation of gases into the liquid–gas interface, diffusion, and surface reactions
180 (Reid and Sayer, 2003). Heterogeneous reaction rates are dependent on relative
181 humidity (RH) (Dentener et al., 1996; Henson et al., 1996; Stutz et al., 2004) because
182 of the significant role of the water film on the aerosol surface in the gas uptake. The
183 formation of ammonium (NH_4^+) is closely related to that of SO_4^{2-} and NO_3^- , as it is
184 resulted from the neutralization of SO_4^{2-} and NO_3^- by dissolved NH_3 in the
185 particulate-phase through aerosol equilibrium treated in ISORROPIA II of Fountoukis
186 and Nenes (2007).

2.2. Missing Heterogeneous Reactions and Their Implementation into Original CMAQ

Heterogeneous chemistry might have played a significant role in the January 2013 haze episode for three reasons. First, the total amount of SO_4^{2-} formed through gas- and aqueous-phase chemistry is too low to explain the observed abrupt increases in the concentrations of SO_4^{2-} by $70\text{--}130\ \mu\text{g m}^{-3}$ within a few hours during the haze episode. The observed concentrations of SO_2 are in the range of $10\text{--}216\ \mu\text{g m}^{-3}$ (Fig. 1). The gas-phase oxidation of SO_2 by OH radicals can convert SO_2 to H_2SO_4 at a maximum rate of $2\% \text{ h}^{-1}$ under sunny conditions, leading to $0.2\text{--}5.5\ \mu\text{g m}^{-3} \text{ h}^{-1}$ H_2SO_4 (which is equivalent to $0.2\text{--}5.4\ \mu\text{g m}^{-3} \text{ h}^{-1}$ SO_4^{2-}). Aqueous-phase chemistry shown in Table 1 can enhance SO_4^{2-} formation in precipitating clouds, which did not occur frequently during the episode. Only two precipitations are recorded in the central China on 20-21 and 30-31 January respectively, which contribute 92% of the total precipitations in January (data derived from <http://cdc.cma.gov.cn>). Meanwhile the weak photochemical activity during dim haze days, characterized by extremely low or even zero O_3 concentrations (He et al., 2014; Y. S. Wang et al., 2014), does not support that gas and aqueous-phase chemistry are dominant pathways for sulfate and nitrate production. As shown in Table 1, the original CMAQ only includes two heterogeneous reactions to produce HNO_3 and does not include any heterogeneous reactions to produce SO_4^{2-} . The original model evaluation against ground-based measurements (as shown in Sect. 4.2.1) shows significant underpredictions of SNA (e.g., normalized mean biases (NMBs) of -40% to -60%). These data analysis and modeling results indicate that the heterogeneous chemistry probably have played a significant role to produce high SNA during the haze pollution. Second, there exist strong correlations between RH and sulfur and nitrogen oxidation ratios (SOR and NOR) during haze in January 2013 (Sun et al., 2014; Y. S. Wang et al., 2014; G. J. Zheng et al., 2014), which resemble the RH-dependence of heterogeneous chemistry. Third, transmission electron microscopy studies have shown that the particles sampled during haze days in the NCP are mostly combined with obvious coatings containing significant sulfur and nitrogen elements, probably generated via some reactions on the particle surfaces (Li and Shao, 2009, 2010; Li et al., 2011). It suggests that surface reactions, probably caused by heterogeneous chemistry, play a significant role in haze formation. Based on the above three reasons, heterogeneous

220 chemistry is regarded as the most important missing reaction pathway and nine new
221 heterogeneous reactions (R16–R24) are then incorporated into CMAQ to improve its
222 capability in reproducing the high SNA concentrations observed during the haze
223 episode through increasing sulfate and nitrate formation. Simulations from the
224 original and the revised CMAQ are compared to study the role of heterogeneous
225 chemistry in producing sulfate and nitrate during this haze episode, which is presented
226 in Sect. 4.2 and 4.3.

227 As shown in Table 1, following the work of K. Wang et al. (2012), nine
228 heterogeneous reactions involving H₂O₂, HNO₃, HO₂, N₂O₅, NO₂, NO₃, O₃, OH, and
229 SO₂ (R16–R24) have been incorporated into original CMAQ. These reactions are
230 assumed to occur on the surface of aerosols. Heterogeneous chemistry is commonly
231 parameterized using a pseudo-first-order rate constant and is assumed to be
232 irreversible (Zhang and Carmichael, 1999; Jacob, 2000). The rate constant k (s⁻¹) for
233 heterogeneous loss of gaseous pollutants is determined by (Jacob, 2000; K. Wang et
234 al., 2012)

235

$$236 \quad k_i = \left(\frac{d_p}{2D_i} + \frac{4}{v_i \gamma_i} \right)^{-1} S_p \quad (1)$$

237

238 where i represents the reactant for heterogeneous reactions, d_p is the effective
239 diameter of the particles (m), D_i is the gas-phase molecular diffusion coefficient for
240 reactant i (m² s⁻¹), v_i is the mean molecular speed of reactant i in the gas phase, γ_i is
241 the uptake coefficient for reactant i (dimensionless), and S_p is the aerosol surface area
242 per unit volume of air (m² m⁻³). The parameters d_p , D_i , v_i , and S_p are calculated in
243 CMAQ, and the parameter γ_i is determined for different reactants based on laboratory
244 measurements reported in the literatures, which is presented below.

245 The values of γ for different gaseous pollutants may vary several orders of
246 magnitude, because of different surface properties, particle compositions,
247 temperature, RH, and laboratory conditions. For a specific combination of particle and
248 gaseous pollutants, the value of γ is highly dependent on RH and increases rapidly as
249 a function of RH (Dentener et al., 1996; Henson et al., 1996; Stutz et al., 2004). For
250 example, Mogili et al. (2006) found that the γ of N₂O₅ increased by a factor of 4 as
251 RH increased in an environmental aerosol chamber. Liu et al. (2008) reported that the
252 γ of HNO₃ on calcium carbonate was enhanced in laboratory experiments by a factor

253 of 15 over a wide range of RHs (from 20–80%). Enhanced γ of HNO₃ with increasing
 254 RH have also been reported on many types of particles including oxides, clay, and
 255 dust. Considering the significant effect of RH on γ , some modeling studies used RH-
 256 dependent γ (Song and Carmichael, 2001; Wei, 2010). For example, Song and
 257 Carmichael (2001) used a value of γ of 0.005 for SO₂ when the RH was lower than
 258 50% and of 0.05 when RH was higher than 50%.

259 The γ for heterogeneous reactions used in this work are determined mainly based
 260 on the work of K. Wang et al. (2012), which used lower and upper limits to represent
 261 a range of γ values reported in the laboratory measurement. On the basis of the lower
 262 and upper limits, we then use a piecewise function to resemble the RH-dependence of
 263 γ . Field measurements during the January 2013 haze episode in Beijing indicate that
 264 the SOR and NOR are highly dependent on RH. They are relatively stable when RH is
 265 lower than 40–50% and rapidly increase when RH is higher. The RH value of 50% is
 266 close to the deliquescence point of particles for a mixture of organic compounds and
 267 ammonium sulfate (Peckhaus et al., 2012), which constitute about 80% of PM_{2.5} in
 268 China (Yang et al., 2011). In this work, we assume the value of γ to be the lower limit
 269 for $RH \leq 50\%$ and that it increases linearly to the upper limit as RH increases to
 270 RH_{\max} , which approximates the correlation between RH and γ . The γ values of the
 271 reactions contributing to sulfate and nitrate (R19–R21, R24) are calculated as the
 272 following equation:

273

$$274 \quad \gamma_i = \begin{cases} \gamma_{low}, RH \in [0, 50\%] \\ \gamma_{low} + (\gamma_{high} - \gamma_{low}) / (RH_{\max} - 0.5) \times (RH - 0.5), RH \in (50\%, RH_{\max}] \\ \gamma_{high}, RH \in (RH_{\max}, 100\%] \end{cases} \quad (2)$$

275

276 where i represents the reactant for heterogeneous reactions, RH_{\max} is the RH value at
 277 which the γ reaches the upper limit, and γ_{low} and γ_{high} are the lower and upper limits of
 278 γ values taken from Table 2 of K. Wang et al. (2012) with one exception for R24.

279 In-situ observations have found significant enhancement of SO₂ oxidation rates
 280 under wet conditions, indicating possible missing heterogeneous reactions on
 281 deliquescent particles (G. J. Zheng et al., 2014). However, the coefficients of SO₂
 282 uptake by aerosols (R24) are only established for ice surfaces and mineral dust
 283 particles (Kolb et al., 2010). As the parameterization of heterogeneous reaction of SO₂
 284 on soot, organics, and SNA aerosols are not well established yet, we first **arbitrarily**

285 **selected** the uptake coefficients from K. Wang et al. (2012) and conducted four
286 sensitivity runs, S1, S2, S3 and S4 by adjusting the uptake coefficients with
287 successive approximation approach. The parameters and evaluations of the four
288 sensitivity runs are presented in supplementary information (Table S1 and Fig. S1).
289 The γ values of the lower and upper limits of SO₂ recommended by K. Wang et al.
290 (2012) are 1.0×10^{-4} and 2.6×10^{-4} , respectively, whereas other works recommended
291 lower γ values for SO₂, e.g., 4.0×10^{-5} in Crowley et al. (2010), 1.35×10^{-5} in Shang
292 et al. (2010), and 0.6×10^{-5} to 2.45×10^{-4} in Wu et al. (2011). We found that using γ
293 in K. Wang et al. (2012) for R24 (sensitivity run S1) will produce unreasonably high
294 sulfate for this haze episode. We finally choose the value from S3 in our work, which
295 can best match observations.

296 We assume the RH_{\max} of sulfate-related heterogeneous reaction (R24) to be
297 100%, and that of nitrate-related heterogeneous reactions (R19–R21) to be 70%. This
298 assumption is made on the basis of the observational result that the SOR increases
299 when the RH rises from 50% to 100% and the NOR increases when the RH rises from
300 50% to 70% and then stays stable when the RH continues to increase. The similar
301 relationship between sulfur (nitrogen) conversion ratios and RH has also been
302 reported in another pollution episode that occurred in the winter of 2011 in Beijing
303 (Sun et al., 2013). For other heterogeneous reactions, we use the mean of lower and
304 upper limit values in the model and assume that they remain constant under different
305 RHs.

306

307 **3. Model Configurations, Simulation Design and Evaluation Protocol**

308 **3.1. Model Configurations and Simulation Design**

309 WRF/CMAQ simulations are performed over East Asia at a horizontal resolution
310 of 36×36 km (see Fig. 2). The simulation period is from 1 to 31 January 2013 with
311 additional 7 days used as a spin-up period to minimize the influence of initial
312 conditions.

313 The physics options selected for the WRF simulation are summarized in Table 2.
314 They are selected based on a number of initial simulations with different option
315 combinations to ensure the best performance for meteorological predictions against
316 observations during this episode. The meteorological initial and boundary conditions

317 (ICs and BCs) are based on the National Centers for Environmental Prediction Final
318 Analysis (NCEP-FNL) reanalysis data. The surface roughness is corrected by
319 increasing the friction velocity by 1.5 times only in the boundary layer scheme to
320 reduce the high biases in wind speed (Mass and Ovens, 2010).

321 The configurations and options used in the CMAQ model are summarized in
322 Table 3. The gas-phase mechanism module is the CB05 gas-phase mechanism with
323 active chlorine chemistry and updated toluene mechanism of Whitten et al. (2010).
324 The aqueous-phase chemistry is based on the updated mechanism of the Regional
325 Acid Deposition Model (RADM) model (Walcek and Taylor, 1986; Chang et al.,
326 1987). The aerosol mechanism applied in this study is the AERO6 aerosol module.
327 The photolytic rates are calculated in-line using simulated aerosols and ozone
328 concentrations. The ICs and BCs are generated from the GEOS-Chem model (Bey et
329 al., 2001).

330 Anthropogenic emissions for China in 2013 used in this work are derived from
331 the MEIC model (Multi-resolution Emission Inventory of China,
332 <http://www.meicmodel.org>). The MEIC model is a dynamic and technology-based
333 emission model developed by Tsinghua University which estimates anthropogenic
334 emissions for about 700 emitting sources over China with unified methodology
335 (Zhang et al., 2007, 2009; Lei et al., 2011a). MEIC model is an update of the bottom-
336 up emission inventory developed by the same group (Zhang et al., 2007, 2009; Lei et
337 al., 2011a) with several updates such as unit-based emission data for power plants (S.
338 W. Wang et al., 2012) and cement plants (Lei et al., 2011b), high-resolution vehicle
339 emission inventory at county level (B. Zheng et al., 2014), and new NMVOC
340 mapping approach for different chemical mechanisms (Li et al., 2014). In the MEIC
341 model, the latest available emission data with real statistics at provincial level is for
342 2012. In this work, emissions for the year of 2013 are used from the extrapolation of
343 the 2012 estimates and updated based on brief statistics at country level.

344 Anthropogenic emissions from the other Asian countries and biomass burning
345 emissions are taken from the MIX emission inventory prepared for the Model Inter-
346 comparison Study Asia Phase III (MICS-ASIA III). Biogenic emissions are calculated
347 by the MEGAN v2.1 (Guenther et al., 2012). Sea salt emission and dust emission are
348 calculated online on the basis of the algorithms developed by Gong (2003) and a
349 physical-based dust emission algorithm FENGSHA
350 (http://www.airqualitymodeling.org/cmaqwiki/index.php?title=CMAQv5.0_Windblo

351 wn_Dust), respectively.

352 Using the WRF/CMAQ modeling system, the impacts of heterogeneous
353 chemistry and the meteorological anomaly of 2013 on the significant production of
354 sulfate and nitrate aerosols during the January 2013 haze episode are investigated with
355 three simulations, as shown in Table 4. The simulation Original CMAQ uses the
356 officially released version of CMAQ v5.0.1. In the simulation Revised CMAQ, nine
357 important heterogeneous reactions are implemented in the model to explore the effects
358 of heterogeneous chemistry. To further evaluate the impacts of the 2013
359 meteorological anomaly on sulfate and nitrate production, another simulation with
360 revised CMAQ is designed to use the same 2013 emissions but with the WRF
361 meteorological predictions for 2012 (Revised CMAQ with 2013Emis&2012Met). The
362 uptake coefficients of heterogeneous chemistry used in the latter two simulations are
363 presented in Table S2 of supplementary information.

364 **3.2. Evaluation Protocol**

365 The model evaluation is performed in terms of domain-wide performance
366 statistics and site-specific temporal variations. The performance statistics are
367 conducted following the evaluation protocol of Zhang et al. (2006, 2011). The
368 statistical parameters include correlation coefficient (R), mean bias (MB), root mean
369 square error (RMSE), NMB, and normalized mean error (NME).

370 Table 5 summarizes the observational datasets used for model evaluation in this
371 study. Three observational datasets are used including the meteorological data from
372 the National Climate Data Center (NCDC), the real-time gaseous and particulate
373 concentrations in 74 cities from the China National Environmental Monitoring Center
374 (CNEMC), and hourly concentrations of chemical species of PM_{2.5} from the ground-
375 based measurement at the Tsinghua University site (THU) located in the northwestern
376 Beijing. The detailed description of these dataset can be found in the supplementary
377 information.

378

379 **4. Results and Discussion**

380 **4.1. Evaluation of Meteorological Predictions**

381 Table 6 presents the statistical performances of the meteorological predictions,

382 including temperature at 2 m (T2), RH at 2 m (RH2), wind speed at 10 m (WS10),
383 wind direction at 10 m (WD10), and daily mean precipitation (Precip). The near-
384 surface temperature agrees reasonably well with observations with MBs of -0.8 °C.
385 Simulated RH2 agrees well with observations across most of China with an NMB of
386 9.9% and an MB of 6.7%. WS10 is overpredicted slightly with an NMB of 9.5% and
387 an MB of 0.3 m s^{-1} for the 36-km domain. The MB of Precip is 1.1 mm and the NMB
388 is 58.8% with a relatively poor performance compared with other meteorological
389 variables. Precip is usually predicted with large biases by meteorological models
390 (Zhang et al., 2011, 2012; L. T. Wang et al., 2014), indicating the limited capability of
391 model to accurately reproduce the precipitating processes. The simulated
392 meteorological variables show generally good agreement with observations, and the
393 overall performances are consistent with similar work conducted for China using the
394 Fifth-Generation Penn State/NCAR Mesoscale Model (MM5) or WRF models (Liu et
395 al., 2010; L. T. Wang et al., 2010, 2014; Zhang et al., 2011; K. Wang et al., 2012; Fu
396 et al., 2014). The simulated meteorological variables agree well with observations in
397 terms of temporal variations and magnitudes at the THU site (as shown in Fig. 3),
398 confirming the reliability of meteorological prediction at location with SNA
399 observation data.

400 **4.2. Chemical Predictions of the Original CMAQ at THU Site**

401 **4.2.1 Sulfate, Nitrate and Ammonium**

402 Figure 4 compares the temporal variations of aerosol compositions in January
403 2013 simulated by the original CMAQ with observation at the THU site, and the
404 statistical performance of the model were summarized in Table 7. Although the
405 original CMAQ model only underpredicts $\text{PM}_{2.5}$ mass concentration by 21.9%, it
406 significantly underpredicts SO_4^{2-} , NO_3^- , and NH_4^+ concentration with NMBs of
407 -54.2% , -40.0% , and -58.1% , respectively. The modeled hourly $\text{PM}_{2.5}$ concentration
408 shows good agreement with the observations when the $\text{PM}_{2.5}$ concentration is below
409 $450 \mu\text{g m}^{-3}$. However, the model failed to predict SNA variations during the polluted
410 days, leading to a large underprediction of total $\text{PM}_{2.5}$ mass concentration during the
411 heavy haze episodes when SNA are dominant compositions in total $\text{PM}_{2.5}$ mass.
412 Figure 5a illustrates the enhancement of SNA in $\text{PM}_{2.5}$ in haze days in January 2013 at
413 THU site. The contribution of SNA to total $\text{PM}_{2.5}$ mass increased from 29.3% to

414 50.3% from clean days to heavily polluted days due to the increased conversion rates
415 of SO₂ and NO₂ under the haze condition (Sun et al., 2013, 2014), while the original
416 CMAQ model could not reproduce the dominant contribution of SNA to PM_{2.5} for
417 those episodes, indicating that some mechanisms that might have significant impacts
418 on SO₄²⁻ and NO₃⁻ formation during haze episodes are absent in the original CMAQ
419 model.

420 As discussed in Sect. 2.2, we believe that heterogeneous chemistry played a key
421 role in sulfate and nitrate production under the haze condition. Nine heterogeneous
422 reactions have been incorporated into the original CMAQ model to improve the
423 model capability in reproducing the observed high concentrations of sulfate and
424 nitrate and study the role of these reactions in the haze pollution. The simulation
425 results from the revised CMAQ with these heterogeneous reactions are described in
426 Sect. 4.3.

427 **4.2.2 Carbonaceous Aerosols**

428 As shown in Fig. 4, the original CMAQ model can generally capture the
429 temporal variation of element carbon at THU site but has a positive bias of 196.2% in
430 monthly mean concentration, implying large overestimation of element carbon
431 emissions in the MEIC inventory for urban Beijing area. The MEIC inventory used in
432 this work is first calculated by province and then allocated to grids by uniformed
433 spatial proxies across provinces, which may induce significant bias for specific
434 locations. Coal boilers and stoves have been phased out from Beijing urban areas and
435 diesel trucks are also prohibited for entering the urban center of Beijing during
436 daytime. These local policies are not considered in MEIC emission inventory, which
437 may lead to the overestimation of element carbon emissions in Beijing urban areas.
438 For organic carbon, the large bias only exists during haze days with mass
439 concentrations larger than 60 µg m⁻³. As the secondary organic aerosols (SOA)
440 module used in CMAQ does not include the formation pathways of heterogeneous
441 reactions involving VOCs and SVOCs, and oligomerization during the haze events
442 and multi-generations of gas-phase oxidations of semi-VOCs (SVOCs), the
443 underestimation is probably caused by the underpredictions in SOA.

444 **4.3. Improvements of SNA Predictions by the Revised CMAQ with** 445 **Heterogeneous Chemistry**

446 Figure 4 compares the temporal variations of $\text{PM}_{2.5}$, SO_4^{2-} , NO_3^- , NH_4^+ , OC, and
447 EC at the THU site simulated by the original and revised CMAQ with observations.
448 The sulfate and nitrate simulations with heterogeneous chemistry are improved
449 significantly in terms of both magnitude and temporal variation. In particular, the
450 significant discrepancies in $\text{PM}_{2.5}$, SO_4^{2-} , NO_3^- and NH_4^+ between the observed and
451 simulated concentrations during severely polluted days are improved, although a
452 couple of observed peak values are still not captured well. The synergic improvement
453 of SNA predictions illustrates the significant role heterogeneous chemistry plays in
454 the haze pollution events. The revised CMAQ shows better performance with NMBs
455 of 0.4%, 6.3%, 5.7%, and -4.1% , for $\text{PM}_{2.5}$, SO_4^{2-} , NO_3^- , and NH_4^+ , respectively. The
456 MBs of sulfate and nitrate are reduced, changing from -17.8 to $2.1 \mu\text{g m}^{-3}$ and from
457 -12.3 to $1.8 \mu\text{g m}^{-3}$, respectively. As expected, the simulated level of $\text{PM}_{2.5}$ is also
458 improved with MBs changing from -40.8 to $0.8 \mu\text{g m}^{-3}$.

459 It should be noted that the revised CMAQ model still significantly
460 underestimated the peak $\text{PM}_{2.5}$ concentration on January 13, 2013. Zheng et al. (2014)
461 argued that the abrupt increase of $\text{PM}_{2.5}$ concentration on January 13 represented rapid
462 recovery from an interruption to the continuous pollution accumulation over the
463 region rather than local chemical production. Our model also failed to predict the high
464 $\text{PM}_{2.5}$ concentration on January 13 over the polluted region (e.g., Langfang and
465 Shijiazhuang, see supplementary information) but agreed well with observation in
466 upwind cities (e.g., Chengde). In this case, the model may have underestimated the
467 regional transport in polluted areas given the fact that the wind speed was
468 underestimated at THU site.

469 The revised CMAQ can capture the enhancement of relative contribution of SNA
470 from clean days to polluted days, as shown in Fig. 5. Observations show that the
471 fractions of SNA increase rapidly to 42.2% and 50.3% on polluted and heavily
472 polluted days, which are well reproduced by the revised CMAQ with fractions of
473 49.0% and 52.6%. For comparison, the original CMAQ gives SNA fractions of 32.1%
474 and 30.8%, which are considerably lower. During polluted and heavily polluted days,
475 there exist significant discrepancies in SNA percentage contributions between the
476 original and revised CMAQ, indicating the important role of heterogeneous chemistry
477 in haze pollution. It should be noted that the good agreement between the revised

478 CMAQ and observations is highly dependent on the selections of uptake coefficients,
479 as discussed in Sect. 2.2. However, all sensitivity runs can reproduce the enhancement
480 of relative contribution of sulfate in haze days (Fig. S1), implying the importance of
481 heterogeneous chemistry. Laboratory measurements of uptake coefficients on the
482 surfaces of mixed and deliquescent aerosols will help to confirm our findings in the
483 future.

484 The evolution patterns of SNA simulated by the revised CMAQ are also
485 generally consistent with other field observations on haze episodes in China, which
486 confirmed the significance of heterogeneous chemistry in haze formation process over
487 China. The enhanced SNA contribution in haze days compared to clean days were
488 also observed in other field campaigns, where the heterogeneous chemistry was
489 attributed as the most probable pathway of observed abrupt increases in SNA aerosols
490 as the oxidation rates of gas-phase and aqueous-phase chemistry were too slow (X. J.
491 Zhao et al., 2013; Ji et al., 2014; Quan et al., 2014; Y. S. Wang et al., 2014). Strong
492 correlations between RH and sulfur and nitrogen oxidation ratios (SOR and NOR)
493 were found during haze episodes (X. Wang et al., 2012; Y. S. Wang et al., 2014; Sun
494 et al., 2014; G. J. Zheng et al., 2014) with sharp increase of SOR and NOR when RH
495 exceeds 50%, lending support to our assumptions in the revised CMAQ.

496 The revised CMAQ gives very similar OC and EC predictions as original
497 CMAQ, with large underpredictions in OC during the haze episodes but
498 overpredictions in EC throughout the simulation period for the reasons discussed
499 previously in Sect. 4.2.2. The percent contributions for EC and OIN are also slightly
500 decreased especially in the polluted and heavily polluted days. This is because the
501 mode-averaging particle diameter is larger due to the enhanced formation of SNA
502 when the heterogeneous reactions are included. The particle settling velocity is
503 increased and thus dry deposition rates are larger, which helps reduce the
504 overpredictions of these species.

505 **4.4. Domain-wide Impact from the Implementation of Heterogeneous** 506 **Chemistry**

507 The simulation results with and without heterogeneous chemistry are compared
508 over the whole domain to evaluate the impact of heterogeneous reactions during the
509 January 2013 haze episode. Table 8 summarizes the statistical performance for surface
510 concentrations of CO, NO₂, SO₂, PM_{2.5}, and PM₁₀ from the simulation with original
511 CMAQ and revised CMAQ for 74 cities in China. The original CMAQ model can

512 generally reproduce the concentrations of aerosol and gaseous pollutants over the
513 whole domain. The model underpredicts the concentrations of CO and PM₁₀ with
514 NMBs of -20.6% and -11.2%, respectively, and overpredicts those of SO₂, NO₂, and
515 PM_{2.5} with NMBs of 51.2%, 13.4%, and 8.1%, respectively. As expected, the
516 overpredictions in SO₂ and NO₂ are improved in the revised CMAQ model because
517 the added heterogeneous reactions enhance their conversions to sulfate and nitrate.
518 The positive biases of SO₂ and NO₂ are reduced from 51.2% to 38.5% and 13.4% to
519 11.2%. We further found that high NMB in SO₂ prediction is mainly contributed by
520 provincial capital cities. As the most developed cities within China, the provincial
521 capital cities tend to prohibit coal use in urban areas or use high-quality coal with low
522 sulfur content, which has not been accurately represented in regional emission
523 inventories which are compiled at the provincial level. As a result, SO₂ emissions
524 from those capital cities may have been overestimated.

525 Figure 6 illustrates the concentration of SNA and PM_{2.5} simulated by the original
526 and revised CMAQ and Fig. 7 further explores the difference in heavily polluted
527 regions. Heterogeneous chemistry enhances SNA concentrations significantly in the
528 most polluted regions in China (the Northeast Plain (NP), NCP, Middle-Lower
529 Yangtze Plain (MLYP), and Sichuan Basin (SB)), leading to the increased PM_{2.5}
530 concentration over those regions. In southern China (e.g., the Pearl River Delta
531 (PRD)), sulfate concentration is still increased but nitrate concentration is decreased
532 by 5–20 μg m⁻³, resulting in a reduction of PM_{2.5} concentration by 10–20 μg m⁻³. The
533 contrasting responses to heterogeneous chemistry in different regions are because of
534 the complex thermodynamic processes of SNA formation, which differ greatly under
535 NH₃-rich and NH₃-poor conditions. The polluted regions listed above (NP, NCP,
536 MLYP, and SB) are all NH₃-rich regions (Wang et al., 2011; B. Zhao et al., 2013), as
537 shown in Fig. 7a, which comprise 24.5% land areas in China but contribute to 47.4%
538 cultivated lands (National Bureau of Statistics, 2013) and 48.3% NH₃ emissions
539 (derived from the MEIC model). The abundant NH₃ emissions provide sufficient
540 amounts of ammonium to neutralize the increased amounts of sulfate and nitrate
541 formed through heterogeneous chemistry; therefore, the total amount of PM_{2.5} in these
542 regions increases with enhancement of both sulfate and nitrate. It causes the positive
543 bias of simulated PM_{2.5} to be larger in the NH₃-rich regions, mainly contributed by the
544 overpredictions of EC and OIN. In southern China, which is an NH₃-poor region in
545 January (Wang et al., 2011), sulfate and nitrate compete for ammonium and the

546 formation of ammonium sulfate occurs first owing to its more thermodynamically
547 stable characteristics, increased levels of sulfate would thus lead to a decrease of
548 nitrate. This phenomenon could even lead to the decrease in the total concentration of
549 PM_{2.5}, because to neutralize with the same amount of ammonium, the mass of sulfate
550 required is smaller than that of nitrate.

551 **4.5. Impact of Meteorology in 2013 on SNA Production**

552 The haze episode in January 2013 was the most serious pollution event in recent
553 years. Why it should happen in 2013 but not in other years is an intriguing question.
554 Emissions of SO₂, NO_x, and PM_{2.5} kept stable during 2011-2013 (derived from the
555 MEIC model), indicating that emissions are not the critical driving force. The
556 anomalous meteorological conditions (low temperature, high RH, and low wind
557 speed) in January 2013 are identified as the key influence factor of haze formation by
558 affecting radiation, horizontal transport, vertical mixing, and the atmospheric reaction
559 rates of air pollutants (Ding and Liu, 2014; Z. F. Wang et al., 2014). As described in
560 Sect. 2.2, meteorological conditions (specifically RH) can affect heterogeneous
561 chemistry by increasing the uptake coefficients of gases. In this section, the impact of
562 the 2013 meteorological conditions on the production of sulfate and nitrate is
563 evaluated using the revised CMAQ with heterogeneous chemistry.

564 The meteorological conditions of 2012 are selected to represent typical weather
565 conditions because they were very close to the 10-year average climatology
566 conditions with regard to temperature, RH, wind speed, and sea level pressure (data
567 derived from <http://cdc.cma.gov.cn>) in the region of the NCP. Figure 8 illustrates the
568 spatial distributions of the monthly mean temperature, RH, PM_{2.5}, sulfate, and nitrate
569 simulated by the revised CMAQ with the meteorological fields of 2012 and 2013. The
570 simulated temperature of 2013 in North and East China is 2–3 °C lower than that in
571 2012 and the simulated RH is 5–25% higher. High RH promotes heterogeneous
572 conversions to generate more sulfate and nitrate and therefore, to increase the total
573 concentration of PM_{2.5}. Significant differences in RH occur in the NCP region, where
574 increases by 15–30% in RH correspond to increases of PM_{2.5} concentration by 70–150
575 μg m⁻³.

576 Traditional chemistry mechanisms play a relatively small role during haze
577 formation because of the low solar radiation and low temperature conditions, and few
578 precipitating clouds, whereas heterogeneous chemistry mechanisms are enhanced by

579 the extremely high RH, which leads to the significant production of sulfate and nitrate
580 aerosols. This provides a perspective to understand how adverse meteorological
581 conditions can affect air quality through reaction pathways that are sensitive to
582 specific meteorological variables. The meteorological anomaly of 2013 occurred not
583 only for temperature and RH, but also for other variables, for example, the shallower
584 PBL and lower wind speed than a typical year. The abnormal changes in these
585 variables also have adverse effects on haze pollution. For example, the height of the
586 PBL across China in 2013 was about 200 m lower than in 2012, which could weaken
587 and confine the vertical mixing of pollutants and thus, aggravate surface pollution.
588 Researches on the impact of these factors have been reported in other studies (e.g., Z.
589 F. Wang et al., 2014; R. H. Zhang et al., 2014).

590

591 **5. Summary and Conclusions**

592 In this work, the WRF/CMAQ has been applied to simulate the January 2013
593 haze episode in China and evaluate the role heterogeneous chemistry played in the
594 formation of sulfate and nitrate during this episode. The simulations with the original
595 and the revised CMAQ are performed and evaluated. In the simulation by original
596 CMAQ, $\text{PM}_{2.5}$, SO_4^{2-} , NO_3^- , and NH_4^+ are underpredicted with NMBs of -21.9% ,
597 -54.2% , -40.0% , and -58.1% , respectively, at the THU site. The incorporation of
598 additional heterogeneous chemistry into CMAQ v5.0.1 significantly improves the
599 model's capability in reproducing sulfate and nitrate concentrations, which are the
600 most important $\text{PM}_{2.5}$ compositions on polluted haze days. The revised CMAQ shows
601 better performances with NMBs of 0.4% , 6.3% , 5.7% , and -4.1% , for $\text{PM}_{2.5}$, SO_4^{2-} ,
602 NO_3^- , and NH_4^+ , respectively, at the THU site. The MBs of sulfate and nitrate are
603 reduced, changing from -17.8 to $2.1 \mu\text{g m}^{-3}$ and from -12.3 to $1.8 \mu\text{g m}^{-3}$,
604 respectively. The revised CMAQ with enhanced heterogeneous chemistry not only
605 captures the magnitude and temporal variation of SNA concentrations, but also
606 reproduces the enhancement of SNA compositions from clean air to polluted haze
607 days, both of which indicate the significantly improved capability of the revised
608 model for haze studies. The revised CMAQ model is then used to evaluate the impact
609 of both heterogeneous chemistry on haze formation during January 2013 and of the
610 meteorological anomaly in 2013 on heterogeneous generation of sulfate and nitrate.

611 Compared with previous studies focusing on the haze episode of January 2013,
612 this work provides a unique method to explore the formation mechanisms of severe

613 haze by evaluating initial application of the original CMAQ, identifying missing
614 heterogeneous chemistry based on model performance, and then incorporating those
615 missing reactions into CMAQ. It thus provides a mechanistic level of understanding
616 of the formation mechanism of the severe regional haze pollution episode.

617 This study has several limitations. First, heterogeneous chemistry is implemented
618 into CMAQ with several assumptions. For example, a pseudo-first-order rate constant
619 is assumed for those reactions and the gas uptake coefficients are assumed to be
620 linearly correlated with RH. Those simplified treatments neglect the effects of
621 complex aerosol compositions and surface uptake, diffusion, and coating and reaction
622 processes, which could inevitably introduce errors and uncertainties in this work (Wei,
623 2010). As a consequence, for example, while the peak concentrations of sulfate and
624 nitrate during the haze pollution event were sharp and occurred during a narrow time
625 window, the revised CMAQ predicts lower and wider spread concentrations. The RH-
626 dependent parameterization of uptake coefficients derived in this work can be refined
627 to consider additional factors, such as temperature, aerosol compositions, amounts of
628 metal catalyst, and surface conditions. In addition, some newly reported
629 heterogeneous reactions, such as SO₂ oxidation promoted by NO_x (He et al., 2014)
630 and OH derived from heterogeneous ClNO₂ production (Sarwar et al., 2014) can
631 enhance SNA but have not yet been included in this work which should be
632 incorporated into CMAQ in the future.

633 Second, there is a lack of sufficient site-specific hourly data for PM_{2.5} and its
634 composition, which are crucial to the model evaluation and improvement. For
635 example, we do not have observation data to evaluate the predicted Fe and Mn in
636 aerosols. The underprediction of Fe and Mn can contribute to the underprediction of
637 sulfate, because the metal catalysis pathway is important for sulfate formation.
638 Although this might not be a critical issue as the model can well predict sulfate
639 concentration in clean days, more observed data for compositions of PM_{2.5} is needed
640 to comprehensively evaluate the model.

641 Finally, the WRF/CMAQ system used in this work is not online-coupled, which
642 does not account for the feedbacks of chemistry and aerosol into meteorology. J.
643 Wang et al. (2014) simulated the same episode using the online-coupled CMAQ and
644 found that including aerosol feedback can increase total aerosol loadings during haze
645 conditions and improve model performance, but lead to larger enhancement of
646 primary aerosols than secondary aerosols, which is opposite to the observations.

647 Online-coupled models with improved chemistry should be developed in the future.
648 Addressing these uncertainties requires an integration of field studies, laboratory
649 experiments, and modeling work by the entire community.

650

651 **Acknowledgements**

652 The work was supported by China's National Basic Research Program
653 (2010CB951803 and 2014CB441301), the National Science Foundation of China
654 (41222036 and 21221004), the Japan International Cooperation Agency, and the U.S.
655 DOE climate modeling programs (DESC0006695) at NCSU, U.S.A. We thank the
656 constructive comments from Dr. Muller and two anonymous reviewers.

657 **References**

658 American Lung Association: 2005 research highlights: health effects of particulate
659 matter and ozone air pollution, [http://www.northeastdiesel.org/pdf/ALA-05-health-](http://www.northeastdiesel.org/pdf/ALA-05-health-studies-biblio.pdf)
660 [studies-biblio.pdf](http://www.northeastdiesel.org/pdf/ALA-05-health-studies-biblio.pdf) (last access: June 2014), 2006.

661
662 Bey, I., Jacob, D. J., Yantosca, R. M., Logan, J. A., Field, B. D., Fiore, A. M., Li, Q.,
663 Liu, H. Y., Mickley, L. J., and Schultz, M. G.: Global modeling of tropospheric
664 chemistry with assimilated meteorology: Model description and evaluation, *J.*
665 *Geophys. Res.-Atmos.*, 106, 23073–23095, doi: 10.1029/2001jd000807, 2001.

666
667 Chang, J. S., Brost, R. A., Isaksen, I. S. A., Madronich, S., Middleton, P., Stockwell,
668 W. R., and Walcek, C. J.: A three-dimensional Eulerian acid deposition model:
669 Physical concepts and formulation, *J. Geophys. Res.-Atmos.*, 92, 14681–14700, doi:
670 10.1029/JD092iD12p14681, 1987.

671
672 Chang, W. L., Bhave, P. V., Brown, S. S., Riemer, N., Stutz, J., and Dabdub, D.:
673 Heterogeneous Atmospheric Chemistry, Ambient Measurements, and Model
674 Calculations of N₂O₅: A Review, *Aerosol. Sci. Tech.*, 45, 665–695, doi:
675 10.1080/02786826.2010.551672, 2011.

676
677 Chou, M.-D., Suarez, M. J., Ho, C.-H., Yan, M. M. H., and Lee, K.-T.:
678 Parameterizations for Cloud Overlapping and Shortwave Single-Scattering Properties
679 for Use in General Circulation and Cloud Ensemble Models, *J. Climate*, 11, 202–214,
680 doi: 10.1175/1520-0442(1998)011<0202:pfcoas>2.0.co;2, 1998.

681
682 Crowley, J. N., Ammann, M., Cox, R. A., Hynes, R. G., Jenkin, M. E., Mellouki, A.,
683 Rossi, M. J., Troe, J., and Wallington, T. J.: Evaluated kinetic and photochemical data
684 for atmospheric chemistry: Volume V – heterogeneous reactions on solid substrates,
685 *Atmos. Chem. Phys.*, 10, 9059–9223, doi: 10.5194/acp-10-9059-2010, 2010.

686
687 Dentener, F. J., Carmichael, G. R., Zhang, Y., Lelieveld, J., and Crutzen, P. J.: Role of
688 mineral aerosol as a reactive surface in the global troposphere, *J. Geophys. Res.-*
689 *Atmos.*, 101, 22869–22889, doi: 10.1029/96jd01818, 1996.

690
691 Ding, Y. H., and Liu, Y. J.: Analysis of long-term variations of fog and haze in China
692 in recent 50 years and their relations with atmospheric humidity, *Sci. China-Earth*
693 *Sci.*, 57, 36–46, doi: 10.1007/s11430-013-4792-1, 2014.

694
695 Fountoukis, C., and Nenes, A.: ISORROPIA II: a computationally efficient
696 thermodynamic equilibrium model for K⁺ - Ca²⁺ - Mg²⁺ - NH₄⁺ - Na⁺ - SO₄²⁻ - NO₃⁻ -
697 Cl⁻ - H₂O aerosols, *Atmos. Chem. Phys.*, 7, 4639–4659, doi: 10.5194/acp-7-4639-
698 2007, 2007.

699

700 Fu, X., Wang, S. X., Cheng, Z., Xing, J., Zhao, B., Wang, J. D., and Hao, J. M.:
701 Source, transport and impacts of a heavy dust event in the Yangtze River Delta, China,
702 in 2011, *Atmos. Chem. Phys.*, 14, 1239–1254, doi: 10.5194/acp-14-1239-2014, 2014.
703

704 Gong, S. L.: A parameterization of sea-salt aerosol source function for sub- and super-
705 micron particles, *Global Biogeochem. Cy.*, 17, 1097, doi: 10.1029/2003gb002079,
706 2003.
707

708 Guenther, A. B., Jiang, X., Heald, C. L., Sakulyanontvittaya, T., Duhl, T., Emmons, L.
709 K., and Wang, X.: The Model of Emissions of Gases and Aerosols from Nature
710 version 2.1 (MEGAN2.1): an extended and updated framework for modeling biogenic
711 emissions, *Geosci. Model Dev.*, 5, 1471–1492, doi: 10.5194/gmd-5-1471-2012, 2012.
712

713 He, H., Wang, Y., Ma, Q., Ma, J., Chu, B., Ji, D., Tang, G., Liu, C., Zhang, H., and
714 Hao, J.: Mineral dust and NO_x promote the conversion of SO₂ to sulfate in heavy
715 pollution days, *Sci. Rep.*, 4, 4172, doi: 10.1038/srep04172, 2014.
716

717 Henson, B. F., Wilson, K. R., and Robinson, J. M.: A physical adsorption model of the
718 dependence of ClONO₂ heterogeneous reactions on relative humidity, *Geophys. Res.*
719 *Lett.*, 23, 1021–1024, doi: 10.1029/96gl00871, 1996.
720

721 Hong, S. Y. and Lim, J. O. J.: The WRF Single-Moment 6-Class Microphysics
722 Scheme (WSM6), *J. Korean Meteor. Soc.*, 42, 129–151,
723 http://www2.mmm.ucar.edu/wrf/users/docs/WSM6-hong_and_lim_JKMS.pdf (last
724 access: June 2014), 2006.
725

726 Jacob, D. J.: Heterogeneous chemistry and tropospheric ozone, *Atmos. Environ.*, 34,
727 2131–2159, doi: 10.1016/S1352-2310(99)00462-8, 2000.
728

729 Ji, D., Li, L., Wang, Y., Zhang, J., Cheng, M., Sun, Y., Liu, Z., Wang, L., Tang, G., Hu,
730 B., Chao, N., Wen, T., and Miao, H.: The heaviest particulate air-pollution episodes
731 occurred in northern China in January, 2013: Insights gained from observation,
732 *Atmos. Environ.*, 92, 546–556, doi:10.1016/j.atmosenv.2014.04.048, 2014.
733

734 Kain, J. S.: The Kain–Fritsch Convective Parameterization: An Update, *J. Appl.*
735 *Meteorol.*, 43, 170–181, doi: 10.1175/1520-0450(2004)043<0170:tkcpau>2.0.co;2,
736 2004.
737

738 Kolb, C. E., Cox, R. A., Abbatt, J. P. D., Ammann, M., Davis, E. J., Donaldson, D. J.,
739 Garrett, B. C., George, C., Griffiths, P. T., Hanson, D. R., Kulmala, M.,
740 McFiggans, G., Pöschl, U., Riipinen, I., Rossi, M. J., Rudich, Y., Wagner, P. E.,
741 Winkler, P. M., Worsnop, D. R., and O' Dowd, C. D.: An overview of current issues
742 in the uptake of atmospheric trace gases by aerosols and clouds, *Atmos. Chem. Phys.*,
743 10, 10561–10605, doi:10.5194/acp-10-10561-2010, 2010.

744
745 Lammel, G., and Leip, A.: Formation of Nitrate and Sulfate in the Plume of Berlin,
746 Environ. Sci. Pollut. R., 12, 213–220, doi: 10.1065/espr2005.03.240, 2005.
747
748 Lei, Y., Zhang, Q., He, K. B., and Streets, D. G.: Primary anthropogenic aerosol
749 emission trends for China, 1990–2005, Atmos. Chem. Phys., 11, 931–954, doi:
750 10.5194/acp-11-931-2011, 2011a.
751
752 Lei, Y., Zhang, Q., Nielsen, C., and He, K.: An inventory of primary air pollutants and
753 CO₂ emissions from cement production in China, 1990–2020, Atmos. Environ., 45,
754 147–154, doi: 10.1016/j.atmosenv.2010.09.034, 2011b.
755
756 Li, M., Zhang, Q., Streets, D. G., He, K. B., Cheng, Y. F., Emmons, L. K., Huo, H.,
757 Kang, S. C., Lu, Z., Shao, M., Su, H., Yu, X., and Zhang, Y.: Mapping Asian
758 anthropogenic emissions of non-methane volatile organic compounds to multiple
759 chemical mechanisms, Atmos. Chem. Phys., 14, 5617–5638, doi:10.5194/acp-14-
760 5617-2014, 2014.
761
762 Li, W., and Shao, L.: Transmission electron microscopy study of aerosol particles
763 from the brown hazes in northern China, J. Geophys. Res.-Atmos., 114, D09302, doi:
764 10.1029/2008jd011285, 2009.
765
766 Li, W., and Shao, L.: Characterization of mineral particles in winter fog of Beijing
767 analyzed by TEM and SEM, Environ. Monit. Assess., 161, 565–573, doi:
768 10.1007/s10661-009-0768-1, 2010.
769
770 Li, W., Zhou, S., Wang, X., Xu, Z., Yuan, C., Yu, Y., Zhang, Q., and Wang, W.:
771 Integrated evaluation of aerosols from regional brown hazes over northern China in
772 winter: Concentrations, sources, transformation, and mixing states, J. Geophys. Res.-
773 Atmos., 116, D09301, doi: 10.1029/2010jd015099, 2011.
774
775 Li, Z., Xia, X., Cribb, M., Mi, W., Holben, B., Wang, P., Chen, H., Tsay, S.-C., Eck, T.
776 F., Zhao, F., Dutton, E. G., and Dickerson, R. E.: Aerosol optical properties and their
777 radiative effects in northern China, J. Geophys. Res.-Atmos., 112, D22S01, doi:
778 10.1029/2006jd007382, 2007.
779
780 Liu, X.-H., Zhang, Y., Cheng, S.-H., Xing, J., Zhang, Q., Streets, D. G., Jang, C.,
781 Wang, W.-X., and Hao, J.-M.: Understanding of regional air pollution over China
782 using CMAQ, part I performance evaluation and seasonal variation, Atmos. Environ.,
783 44, 2415–2426, doi: 10.1016/j.atmosenv.2010.03.035, 2010.
784
785 Liu, Y., Gibson, Cain, Wang, H., Grassian, and Laskin, A.: Kinetics of Heterogeneous
786 Reaction of CaCO₃ Particles with Gaseous HNO₃ over a Wide Range of Humidity, J.
787 Phys. Chem. A, 112, 1561–1571, doi: 10.1021/jp076169h, 2008.

788

789 Mass, C., and Ovens, D.: WRF Model Physics: Progress, Problems, and Perhaps
790 Some Solutions, The 11th WRF Users' Workshop, 21–25 June, NCAR Center Green
791 Campus,

792 [http://www.mmm.ucar.edu/wrf/users/workshops/WS2010/presentations/session%204/
793 4-1_WRFworkshop2010Final.pdf](http://www.mmm.ucar.edu/wrf/users/workshops/WS2010/presentations/session%204/4-1_WRFworkshop2010Final.pdf) (last access: June 2014), 2010.

794

795 McNaughton, C. S., Clarke, A. D., Kapustin, V., Shinozuka, Y., Howell, S. G.,
796 Anderson, B. E., Winstead, E., Dibb, J., Scheuer, E., Cohen, R. C., Wooldridge, P.,
797 Perring, A., Huey, L. G., Kim, S., Jimenez, J. L., Dunlea, E. J., DeCarlo, P. F.,
798 Wennberg, P. O., Crouse, J. D., Weinheimer, A. J., and Flocke, F.: Observations of
799 heterogeneous reactions between Asian pollution and mineral dust over the Eastern
800 North Pacific during INTEX-B, *Atmos. Chem. Phys.*, 9, 8283–8308, doi:
801 10.5194/acp-9-8283-2009, 2009.

802

803 Mercado, L. M., Bellouin, N., Sitch, S., Boucher, O., Huntingford, C., Wild, M., and
804 Cox, P. M.: Impact of changes in diffuse radiation on the global land carbon sink,
805 *Nature*, 458, 1014–1017, doi: 10.1038/nature07949, 2009.

806

807 Mlawer, E. J., Taubman, S. J., Brown, P. D., Iacono, M. J., and Clough, S. A.:
808 Radiative transfer for inhomogeneous atmospheres: RRTM, a validated correlated-k
809 model for the longwave, *J. Geophys. Res.-Atmos.*, 102, 16663–16682, doi:
810 10.1029/97jd00237, 1997.

811

812 Mogili, P. K., Kleiber, P. D., Young, M. A., and Grassian, V. H.: N₂O₅ hydrolysis on
813 the components of mineral dust and sea salt aerosol: Comparison study in an
814 environmental aerosol reaction chamber, *Atmos. Environ.*, 40, 7401–7408, doi:
815 10.1016/j.atmosenv.2006.06.048, 2006.

816

817 National Bureau of Statistics: China Statistical Yearbook 2013, China Statistics Press,
818 Beijing, 2013.

819

820 Peckhaus, A., Grass, S., Treuel, L., and Zellner, R.: Deliquescence and Efflorescence
821 Behavior of Ternary Inorganic/Organic/Water Aerosol Particles, *J. Phys. Chem. A*,
822 116, 6199–6210, doi: 10.1021/jp211522t, 2012.

823

824 Pleim, J. E.: A Combined Local and Nonlocal Closure Model for the Atmospheric
825 Boundary Layer. Part I: Model Description and Testing, *J. Appl. Meteorol. Clim.*, 46,
826 1383–1395, doi: 10.1175/jam2539.1, 2007.

827

828 Quan, J., Tie, X., Zhang, Q., Liu, Q., Li, X., Gao, Y., and Zhao, D.: Characteristics of
829 heavy aerosol pollution during the 2012–2013 winter in Beijing, China, *Atmos.*
830 *Environ.*, 88, 83–89, doi: 10.1016/j.atmosenv.2014.01.058, 2014.

831

832 Ravishankara, A. R.: Heterogeneous and Multiphase Chemistry in the Troposphere,
833 Science, 276, 1058–1065, doi: 10.1126/science.276.5315.1058, 1997.
834

835 Reid, J. P., and Sayer, R. M.: Heterogeneous atmospheric aerosol chemistry:
836 laboratory studies of chemistry on water droplets, Chem. Soc. Rev., 32, 70–79, doi:
837 10.1039/b204463n, 2003.
838

839 Sarwar, G., Simon, H., Xing, J., and Mathur, R.: Importance of tropospheric ClNO₂
840 chemistry across the Northern Hemisphere, Geophys. Res. Lett., 41, 4050–4058, doi:
841 10.1002/2014GL059962, 2014.
842

843 Schumann, U., and Huntrieser, H.: The global lightning-induced nitrogen oxides
844 source, Atmos. Chem. Phys., 7, 3823–3907, doi: 10.5194/acp-7-3823-2007, 2007.
845

846 Seinfeld, J. H., Carmichael, G. R., Arimoto, R., Conant, W. C., Brechtel, F. J., Bates,
847 T. S., Cahill, T. A., Clarke, A. D., Doherty, S. J., Flatau, P. J., Huebert, B. J., Kim, J.,
848 Markowicz, K. M., Quinn, P. K., Russell, L. M., Russell, P. B., Shimizu, A.,
849 Shinozuka, Y., Song, C. H., Tang, Y., Uno, I., Vogelmann, A. M., Weber, R. J., Woo,
850 J.-H., and Zhang, X. Y.: ACE-ASIA: Regional Climatic and Atmospheric Chemical
851 Effects of Asian Dust and Pollution, B. Am. Meteorol. Soc., 85, 367–380, doi:
852 10.1175/bams-85-3-367, 2004.
853

854 Shang, J., Li, J., and Zhu, T.: Heterogeneous reaction of SO₂ on TiO₂ particles, Sci.
855 China Chem., 53, 2637–2643, doi: 10.1007/s11426-010-4160-3, 2010.
856

857 Song, C. H., and Carmichael, G. R.: A three-dimensional modeling investigation of
858 the evolution processes of dust and sea-salt particles in east Asia, J. Geophys. Res.-
859 Atmos., 106, 18131–18154, doi: 10.1029/2000jd900352, 2001.
860

861 Stutz, J., Alicke, B., Ackermann, R., Geyer, A., Wang, S., White, A. B., Williams, E.
862 J., Spicer, C. W., and Fast, J. D.: Relative humidity dependence of HONO chemistry
863 in urban areas, J. Geophys. Res.-Atmos., 109, D03307, doi: 10.1029/2003jd004135,
864 2004.
865

866 Sun, Y., Zhuang, G., Tang, A., Wang, Y., and An, Z.: Chemical Characteristics of
867 PM_{2.5} and PM₁₀ in Haze–Fog Episodes in Beijing, Environ. Sci. Technol., 40, 3148–
868 3155, doi: 10.1021/es051533g, 2006.
869

870 Sun, Y., Wang, Z., Fu, P., Jiang, Q., Yang, T., Li, J., and Ge, X.: The impact of relative
871 humidity on aerosol composition and evolution processes during wintertime in
872 Beijing, China, Atmos. Environ., 77, 927–934, doi: 10.1016/j.atmosenv.2013.06.019,
873 2013.
874

875 Sun, Y., Jiang, Q., Wang, Z., Fu, P., Li, J., Yang, T., and Yin, Y.: Investigation of the

876 Sources and Evolution Processes of Severe Haze Pollution in Beijing in January 2013,
877 *J. Geophys. Res.-Atmos.*, 119, 4380–4398, doi:10.1002/2014jd021641, 2014.
878
879 Usher, C. R., Michel, A. E., and Grassian, V. H.: Reactions on Mineral Dust, *Chem.*
880 *Rev.*, 103, 4883–4940, doi: 10.1021/cr020657y, 2003.
881
882 Walcek, C. J., and Taylor, G. R.: A Theoretical Method for Computing Vertical
883 Distributions of Acidity and Sulfate Production within Cumulus Clouds, *J. Atmos.*
884 *Sci.*, 43, 339–355, doi: 10.1175/1520-0469(1986)043<0339:atmfcv>2.0.co;2, 1986.
885
886 Wang, J., Wang, S., Jiang, J., Ding, A., Zheng, M., Zhao, B., Wong, D. C., Zhou, W.,
887 Zheng, G., Wang, L., Pleim, J. E., and Hao, J.: Impact of aerosol–meteorology
888 interactions on fine particle pollution during China’s severe haze episode in January
889 2013, *Environ. Res. Lett.*, 9, doi: 10.1088/1748-9326/9/9/094002, 2014.
890
891 Wang, K., Zhang, Y., Nenes, A., and Fountoukis, C.: Implementation of dust emission
892 and chemistry into the Community Multiscale Air Quality modeling system and initial
893 application to an Asian dust storm episode, *Atmos. Chem. Phys.*, 12, 10209–10237,
894 doi: 10.5194/acp-12-10209-2012, 2012.
895
896 Wang, L. T., Jang, C., Zhang, Y., Wang, K., Zhang, Q., Streets, D., Fu, J., Lei, Y.,
897 Schreifels, J., He, K., Hao, J., Lam, Y.-F., Lin, J., Meskhidze, N., Voorhees, S., Everts,
898 D., and Phillips, S.: Assessment of air quality benefits from national air pollution
899 control policies in China. Part I: Background, emission scenarios and evaluation of
900 meteorological predictions, *Atmos. Environ.*, 44, 3442–3448, doi:
901 10.1016/j.atmosenv.2010.05.051, 2010.
902
903 Wang, L. T., Wei, Z., Yang, J., Zhang, Y., Zhang, F. F., Su, J., Meng, C. C., and Zhang,
904 Q.: The 2013 severe haze over southern Hebei, China: model evaluation, source
905 apportionment, and policy implications, *Atmos. Chem. Phys.*, 14, 3151–3173,
906 doi:10.5194/acp-14-3151-2014, 2014.
907
908 Wang, S., Xing, J., Jang, C., Zhu, Y., Fu, J. S., and Hao, J.: Impact Assessment of
909 Ammonia Emissions on Inorganic Aerosols in East China Using Response Surface
910 Modeling Technique, *Environ. Sci. Technol.*, 45, 9293–9300, doi:
911 10.1021/es2022347, 2011.
912
913 Wang, S. W., Zhang, Q., Streets, D. G., He, K. B., Martin, R. V., Lamsal, L. N., Chen,
914 D., Lei, Y., and Lu, Z.: Growth in NO_x emissions from power plants in China:
915 bottom-up estimates and satellite observations, *Atmos. Chem. Phys.*, 12, 4429–4447,
916 doi: 10.5194/acp-12-4429-2012, 2012.
917
918 Wang, X., Wang, W., Yang, L., Gao, X., Nie, W., Yu, Y., Xu, P., Zhou, Y., and Wang,
919 Z.: The secondary formation of inorganic aerosols in the droplet mode through

920 heterogeneous aqueous reactions under haze conditions, *Atmos. Environ.*, *63*, 68–76,
921 doi: 10.1016/j.atmosenv.2012.09.029, 2012.

922

923 Wang, Y., Zhuang, G., Sun, Y., and An, Z.: The variation of characteristics and
924 formation mechanisms of aerosols in dust, haze, and clear days in Beijing, *Atmos.*
925 *Environ.*, *40*, 6579–6591, doi: 10.1016/j.atmosenv.2006.05.066, 2006.

926

927 Wang, Y. S., Yao, L., Wang, L. L., Liu, Z. R., Ji, D. S., Tang, G. Q., Zhang, J. K., Sun,
928 Y., Hu, B., and Xin, J. Y.: Mechanism for the formation of the January 2013 heavy
929 haze pollution episode over central and eastern China, *Sci. China-Earth Sci.*, *57*, 14–
930 25, doi: 10.1007/s11430-013-4773-4, 2014.

931

932 Wang, Z. F., Li, J., Wang, Z., Yang, W. Y., Tang, X., Ge, B. Z., Yan, P. Z., Zhu, L. L.,
933 Chen, X. S., Chen, H. S., Wang, W., Li, J. J., Liu, B., Wang, X. Y., Wand, W., Zhao, Y.
934 L., Lu, N., and Su, D. B.: Modeling study of regional severe hazes over mid-eastern
935 China in January 2013 and its implications on pollution prevention and control, *Sci.*
936 *China-Earth Sci.*, *57*, 3–13, doi: 10.1007/s11430-013-4793-0, 2014.

937

938 Wei, C.: Modeling the effects of heterogeneous reactions on atmospheric chemistry
939 and aerosol properties, PhD Diss., University of Iowa, <http://ir.uiowa.edu/etd/903> (last
940 access: June 2014), 2010.

941

942 Whitten, G. Z., Heo, G., Kimura, Y., McDonald-Buller, E., Allen, D. T., Carter, W. P.
943 L., and Yarwood, G.: A new condensed toluene mechanism for Carbon Bond: CB05-
944 TU, *Atmos. Environ.*, *44*, 5346–5355, doi: 10.1016/j.atmosenv.2009.12.029, 2010.

945

946 Wu, L. Y., Tong, S. R., Wang, W. G., and Ge, M. F.: Effects of temperature on the
947 heterogeneous oxidation of sulfur dioxide by ozone on calcium carbonate, *Atmos.*
948 *Chem. Phys.*, *11*, 6593–6605, doi: 10.5194/acp-11-6593-2011, 2011.

949

950 Xiu, A., and Pleim, J. E.: Development of a Land Surface Model. Part I: Application
951 in a Mesoscale Meteorological Model, *J. Appl. Meteorol.*, *40*, 192–209, doi:
952 10.1175/1520-0450(2001)040<0192:doalsm>2.0.co;2, 2001.

953

954 Yang, F., Tan, J., Zhao, Q., Du, Z., He, K., Ma, Y., Duan, F., and Chen, G.:
955 Characteristics of PM_{2.5} speciation in representative megacities and across China,
956 *Atmos. Chem. Phys.*, *11*, 5207–5219, doi: 10.5194/acp-11-5207-2011, 2011.

957

958 Yang, K., Dickerson, R. R., Carn, S. A., Ge, C., and Wang, J.: First observations of
959 SO₂ from the satellite Suomi NPP OMPS: Widespread air pollution events over
960 China, *Geophys. Res. Lett.*, *40*, 4957–4962, doi: 10.1002/grl.50952, 2013.

961

962 Zhang, J. K., Sun, Y., Liu, Z. R., Ji, D. S., Hu, B., Liu, Q., and Wang, Y. S.:
963 Characterization of submicron aerosols during a month of serious pollution in Beijing,

964 2013, *Atmos. Chem. Phys.*, 14, 2887–2903, doi: 10.5194/acp-14-2887-2014, 2014.
965
966 Zhang, Q., Streets, D. G., He, K., Wang, Y., Richter, A., Burrows, J. P., Uno, I., Jang,
967 C. J., Chen, D., Yao, Z., and Lei, Y.: NO_x emission trends for China, 1995–2004: The
968 view from the ground and the view from space, *J. Geophys. Res.-Atmos.*, 112,
969 D22306, doi: 10.1029/2007jd008684, 2007.
970
971 Zhang, Q., Streets, D. G., Carmichael, G. R., He, K. B., Huo, H., Kannari, A.,
972 Klimont, Z., Park, I. S., Reddy, S., Fu, J. S., Chen, D., Duan, L., Lei, Y., Wang, L. T.,
973 and Yao, Z. L.: Asian emissions in 2006 for the NASA INTEX-B mission, *Atmos.*
974 *Chem. Phys.*, 9, 5131–5153, doi: 10.5194/acp-9-5131-2009, 2009.
975
976 Zhang, R. H., Li, Q., and Zhang, R. N.: Meteorological conditions for the persistent
977 severe fog and haze event over eastern China in January 2013, *Sci. China-Earth Sci.*,
978 57, 26–35, doi: 10.1007/s11430-013-4774-3, 2014.
979
980 Zhang, Y., and Carmichael, G. R.: The Role of Mineral Aerosol in Tropospheric
981 Chemistry in East Asia—A Model Study, *J. Appl. Meteorol.*, 38, 353–366, doi:
982 10.1175/1520-0450(1999)038<0353:tromai>2.0.co;2, 1999.
983
984 Zhang, Y., Sunwoo, Y., Kotamarthi, V., and Carmichael, G. R.: Photochemical
985 Oxidant Processes in the Presence of Dust: An Evaluation of the Impact of Dust on
986 Particulate Nitrate and Ozone Formation, *J. Appl. Meteorol.*, 33, 813–824, doi:
987 10.1175/1520-0450(1994)033<0813:popitp>2.0.co;2, 1994.
988
989 Zhang, Y., Liu, P., Pun, B., and Seigneur, C.: A comprehensive performance
990 evaluation of MM5-CMAQ for the Summer 1999 Southern Oxidants Study episode—
991 Part I: Evaluation protocols, databases, and meteorological predictions, *Atmos.*
992 *Environ.*, 40, 4825–4838, doi: 10.1016/j.atmosenv.2005.12.043, 2006.
993
994 Zhang, Y., Cheng, S.-H., Chen, Y.-S., and Wang, W.-X.: Application of MM5 in
995 China: Model evaluation, seasonal variations, and sensitivity to horizontal grid
996 resolutions, *Atmos. Environ.*, 45, 3454–3465, doi: 10.1016/j.atmosenv.2011.03.019,
997 2011.
998
999 Zhang, Y., Chen, Y., Sarwar, G., and Schere, K.: Impact of gas-phase mechanisms on
1000 Weather Research Forecasting Model with Chemistry (WRF/Chem) predictions:
1001 Mechanism implementation and comparative evaluation, *J. Geophys. Res.-Atmos.*,
1002 117, D01301, doi: 10.1029/2011jd015775, 2012.
1003
1004 Zhao, B., Wang, S., Wang, J., Fu, J. S., Liu, T., Xu, J., Fu, X., and Hao, J.: Impact of
1005 national NO_x and SO₂ control policies on particulate matter pollution in China,
1006 *Atmos. Environ.*, 77, 453–463, doi: 10.1016/j.atmosenv.2013.05.012, 2013.
1007

1008 Zhao, P., Zhang, X., Xu, X., and Zhao, X.: Long-term visibility trends and
1009 characteristics in the region of Beijing, Tianjin, and Hebei, China, *Atmos. Res.*, 101,
1010 711–718, doi: 10.1016/j.atmosres.2011.04.019, 2011.

1011 Zhao, X. J., Zhao, P. S., Xu, J., Meng, W., Pu, W. W., Dong, F., He, D., and Shi, Q. F.:
1012 Analysis of a winter regional haze event and its formation mechanism in the North
1013 China Plain, *Atmos. Chem. Phys.*, 13, 5685–5696, doi: 10.5194/acp-13-5685-2013,
1014 2013.

1015

1016 Zhao, Y., Duan, L., Xing, J., Larssen, T., Nielsen, C. P., and Hao, J.: Soil Acidification
1017 in China: Is Controlling SO₂ Emissions Enough?, *Environ. Sci. Technol.*, 43, 8021–
1018 8026, doi: 10.1021/es901430n, 2009.

1019

1020 Zheng, B., Huo, H., Zhang, Q., Yao, Z. L., Wang, X. T., Yang, X. F., Liu, H., and He,
1021 K. B.: High-resolution mapping of vehicle emissions in China in 2008, *Atmos. Chem.*
1022 *Phys.*, 14, 9787–9805, doi:10.5194/acp-14-9787-2014, 2014.

1023

1024 Zheng, G. J., Duan, F. K., Ma, Y. L., Cheng, Y., Zheng, B., Zhang, Q., Huang, T.,
1025 Kimoto, T., Chang, D., Su, H., Pöschl, U., Cheng, Y. F., and He, K. B.: Exploring the
1026 severe winter haze in Beijing, *Atmos. Chem. Phys. Discuss.*, 14, 17907–17942,
1027 doi:10.5194/acpd-14-17907-2014, 2014.

1028

1029 Table 1. Main reactions contributing to sulfate and nitrate production in original
 1030 CMAQ and heterogeneous reactions newly added in revised CMAQ

Type	Reaction #.	Reaction	Contributions to PM _{2.5}
original CMAQ			
Gas-phase chemistry (All species in gas phase)	R1	$\text{SO}_2 + \text{OH} + \text{H}_2\text{O} + \text{O}_2 \rightarrow \text{H}_2\text{SO}_4 + \text{HO}_2$	Sulfate
	R2	$\text{NO}_2 + \text{OH} \rightarrow \text{HNO}_3$	Nitrate
	R3	$\text{N}_2\text{O}_5 + \text{H}_2\text{O} \rightarrow 2\text{HNO}_3$	Nitrate
	R4	$\text{NO}_3 + \text{HO}_2 \rightarrow \text{HNO}_3 + \text{O}_2$	Nitrate
	R5	$\text{NTR}^a + \text{OH} \rightarrow \text{HNO}_3$	Nitrate
	R6	$\text{NO}_3 + \text{VOCs}^b \rightarrow \text{HNO}_3$	Nitrate
Aqueous-phase kinetic chemistry (All species in aqueous phase)	R7	$\text{HSO}_3^- + \text{H}_2\text{O}_2 \rightarrow \text{SO}_4^{2-} + \text{H}^+ + \text{H}_2\text{O}$	Sulfate
	R8	$\text{HSO}_3^- + \text{MHP}^c \rightarrow \text{SO}_4^{2-} + \text{H}^+$	Sulfate
	R9	$\text{HSO}_3^- + \text{PAA}^d \rightarrow \text{SO}_4^{2-} + \text{H}^+$	Sulfate
	R10	$\text{SO}_2 + \text{O}_3 + \text{H}_2\text{O} \rightarrow \text{SO}_4^{2-} + 2\text{H}^+ + \text{O}_2$	Sulfate
	R11	$\text{HSO}_3^- + \text{O}_3 \rightarrow \text{SO}_4^{2-} + \text{H}^+ + \text{O}_2$	Sulfate
	R12	$\text{SO}_3^{2-} + \text{O}_3 \rightarrow \text{SO}_4^{2-} + \text{O}_2$	Sulfate
	R13	$\text{SO}_2 + \text{H}_2\text{O} + 0.5\text{O}_2 + \text{Fe(III)/Mn(II)} \rightarrow \text{SO}_4^{2-} + 2\text{H}^+$	Sulfate
Heterogeneous chemistry ^e	R14	$\text{N}_2\text{O}_5 (\text{g}) + \text{H}_2\text{O} (\text{aq}) \rightarrow 2\text{HNO}_3 (\text{aq})$ $2\text{NO}_2 (\text{g}) + \text{H}_2\text{O} (\text{aq}) \rightarrow \text{HONO} (\text{aq}) + \text{HNO}_3 (\text{aq})$	Nitrate
	R15		Nitrate
revised CMAQ			
Newly added heterogeneous chemistry	R16	$\text{H}_2\text{O}_2 (\text{g}) + \text{Aerosol} \rightarrow \text{Products}$	Affect R7
	R17	$\text{HNO}_3 (\text{g}) + \text{Aerosol} \rightarrow 0.5\text{NO}_3^- + 0.5\text{NO}_x (\text{g})$	Renoxification
	R18	$\text{HO}_2 (\text{g}) + \text{Fe(II)} \rightarrow \text{Fe(III)} + \text{H}_2\text{O}_2$	Affect R4 and R7
	R19	$\text{N}_2\text{O}_5 (\text{g}) + \text{Aerosol} \rightarrow 2\text{NO}_3^-$	Nitrate
	R20	$\text{NO}_2 (\text{g}) + \text{Aerosol} \rightarrow \text{NO}_3^-$	Nitrate
	R21	$\text{NO}_3 (\text{g}) + \text{Aerosol} \rightarrow \text{NO}_3^-$	Nitrate
	R22	$\text{O}_3 (\text{g}) + \text{Aerosol} \rightarrow \text{Products}$	Affect R10–R12
	R23	$\text{OH} (\text{g}) + \text{Aerosol} \rightarrow \text{Products}$	Affect R1–R2, R5
	R24	$\text{SO}_2 (\text{g}) + \text{Aerosol} \rightarrow \text{SO}_4^{2-}$	Sulfate

1031 ^a NTR: organic nitrate.

1032 ^b VOCs include: formaldehyde, acetaldehyde, propionaldehyde and higher aldehydes, cresol and higher
 1033 molecular weight phenols, nitro cresol, aromatic ring open products, and isoprene oxidation products.

1034 ^c MHP: methylhydroperoxide.

1035 ^d PAA: peroxyacetic acid.

1036 ^e R14 and R15 were removed after R16-R24 were added into the model.

1037

Table 2. Domain, configurations, and major physical options used in WRF v3.5.1

Simulation period	Dec 2012 and Jan 2013
Domain	East Asia (Columns:178, Rows: 133) with 3 extra grids in each boundary of Domain 1 (Columns:172, Rows: 127)
Horizontal resolution	36 km
Vertical resolution	23 sigma levels from surface to tropopause (about 100 mb)
Meteorological IC and BC	Reanalysis data from the National Centers for Environmental Prediction Final Analysis (NCEP-FNL)
Shortwave radiation	New Goddard scheme (Chou et al., 1998)
Longwave radiation	The rapid radiative transfer model (RRTM) (Mlawer et al., 1997)
Land surface model	The USGS 24-category land use data
Surface layer	Pleim-Xiu land surface scheme (Xiu and Pleim, 2001)
Planetary boundary layer model	ACM2 PBL scheme (Pleim, 2007)
Cumulus parameterization	Kain-Fritsch cumulus scheme (Kain, 2004)
Cloud microphysics	WSM6 (Hong and Lim, 2006)
Analysis nudging	Temperature and water vapor mixing (above PBL); wind (in and above PBL)
Observational nudging	Temperature, water vapor mixing and wind (in and above PBL)
Soil nudging	Include soil moisture and temperature
FDDA data	NCEP Automated Data Processing (ADP) surface (ds461.0) and upper (ds351.0) air data

Table 3. Domain, configurations, and options used in CMAQ v5.0.1

Simulation period	25 Dec 2012 to 31 Jan 2013
Domain	Domain 1 (Columns:172, Rows: 127)
Horizontal resolution	36 km
Vertical resolution	14 sigma levels from surface to tropopause. The values of sigma levels are: 1.000, 0.995, 0.988, 0.980, 0.970, 0.956, 0.938, 0.893, 0.839, 0.777, 0.702, 0.582, 0.400, 0.200, and 0.000.
IC and BC	GEOS-Chem 2° × 2.5° global simulation
Gas-phase mechanism	CB05 gas-phase mechanism with active chlorine chemistry and updated toluene mechanism of Whitten et al. (2010)
Aqueous-phase mechanism	The updated mechanism of the RADM model (Walcek and Taylor, 1986; Chang et al., 1987)
Aerosol module	AERO6
Photolytic rate	Calculate photolytic rates in-line using simulated aerosols and ozone concentrations
Cloud module	ACM cloud processor that uses the ACM methodology to compute convective mixing for AERO6
Windblown dust	The physical-based dust emission algorithm FENGSHA (http://www.airqualitymodeling.org/cmaqwiki/index.php?title=CMAQv5.0_Windblown_Dust)
Lightning NO _x	Not included, due to extremely low flash rates over the East Asia in winter (Schumann and Huntrieser, 2007)

1040

Table 4. Simulation design

Run Index	Emission	Meteorology	Model configuration	Purpose
Original CMAQ	Jan. 2013	Jan. 2013	original CMAQ	Examine the capability and limitation of the original model to study severe haze pollution
Revised CMAQ	Jan. 2013	Jan. 2013	revised CMAQ with heterogeneous chemistry	Evaluate the role of heterogeneous chemistry in haze pollution
Revised CMAQ with 2013Emis&2012Met	Jan. 2013	Jan. 2012	revised CMAQ with heterogeneous chemistry	Evaluate the impact of meteorological anomaly of 2013 on sulfate and nitrate production

1041

1042

Table 5. Observational data for model evaluation.

Dataset	Data	Variable ^d	Frequency	Site number	Time period	Sources
NCDC ^a	Meteorology	T2, RH2, WS10, WD10, Precip	Every 1 or 3 h	~1000	1–31 Jan 2013	ftp://ftp.ncdc.noaa.gov/pub/data/noaa/
CNEMC ^b	Gaseous and particulate species	SO ₂ , NO ₂ , CO, PM _{2.5} , and PM ₁₀	Hourly	496	1–31 Jan 2013	http://113.108.142.147:20035/emcpublish/
THU ^c	Particulate species	PM _{2.5} , SO ₄ ²⁻ , NO ₃ ⁻ , NH ₄ ⁺ , EC, OC	Hourly	1	1–31 Jan 2013	G. J. Zheng et al. (2014)

1043 ^a NCDC: Meteorological data obtained from the National Climate Data Center.1044 ^b CNEMC: Gaseous and particulate concentrations obtained from the China National Environmental
1045 Monitoring Center.1046 ^c THU: Particulate species concentration measured at Tsinghua University.1047 ^d T2: Temperature at 2 m; RH2: Relative humidity at 2 m; WS10: wind speed at 10 m; WD10: wind
1048 direction at 10 m; Precip: daily Precipitation.

1049

1050

Table 6. Performance statistics of WRF simulation

	T2 ^a	RH2 ^a	WS10 ^a	WD10 ^a	Precip ^a
Data pairs ^b	385753	385103	385165	336507	488
MeanObs ^b	-0.2	67.5	2.7	227.1	1.8
MeanSim ^b	-1.1	74.1	3.0	205.6	2.9
R ^b	1.0	0.7	0.6	0.3	0.4
MB ^b	-0.8	6.7	0.3	-21.6	1.1
RMSE ^b	3.5	14.9	2.1	177.2	7.9
NMB(%) ^b	-389.5	9.9	9.5	-9.5	58.8
NME(%) ^b	1211.3	17	57.9	41.9	145

1051 ^a Definitions of these variables can be found in the footnotes of Table 5. The units of T2, RH2, WS10,
 1052 WD10, and Precip are °C, %, m s⁻¹, degree, and mm day⁻¹, respectively. The T2, RH2, WS10 and
 1053 WD10 are evaluated using hourly data and the Precip is evaluated using daily data.

1054 ^b Data pairs: the number of observed and simulated data pairs; MeanObs: mean observational data;
 1055 MeanSim: mean simulation results; R: correlation coefficient; MB: mean bias; RMSE: root mean
 1056 square error; NMB: normalized mean bias; NME: normalized mean error.

1057 Table 7. Performance statistics of the original and revised CMAQ model at the THU
 1058 site

		PM _{2.5} ^a	SO ₄ ²⁻	NO ₃ ⁻	NH ₄ ⁺	EC	OC
Obs		186.0	32.8	30.7	20.8	4.2	47.3
Original CMAQ	MeanSim	145.2	15.0	18.4	8.7	12.3	35.3
	R	0.8	0.6	0.8	0.7	0.6	0.8
	MB	-40.8	-17.8	-12.3	-12.1	8.2	-12.0
	RMSE	102.3	30.5	19.6	18.5	9.0	19.9
	NMB(%)	-21.9	-54.2	-40.0	-58.1	196.2	-25.3
	NME(%)	33.8	57.4	42.0	59.0	196.2	29.2
Revised CMAQ	MeanSim	186.8	34.8	32.4	19.9	11.8	34.2
	R	0.8	0.7	0.8	0.8	0.6	0.7
	MB	0.8	2.1	1.8	-0.8	7.6	-13.1
	RMSE	83.3	21.2	14.6	11.6	8.4	21.2
	NMB(%)	0.4	6.3	5.7	-4.1	183.0	-27.8
	NME(%)	33.1	46.8	35.3	39.4	183.8	31.7

1059 ^a The units of PM_{2.5}, SO₄²⁻, NO₃⁻, NH₄⁺, OC, and EC are all μg m⁻³.

1060

1061 Table 8. Domain-wide performance statistics of the original and revised CMAQ

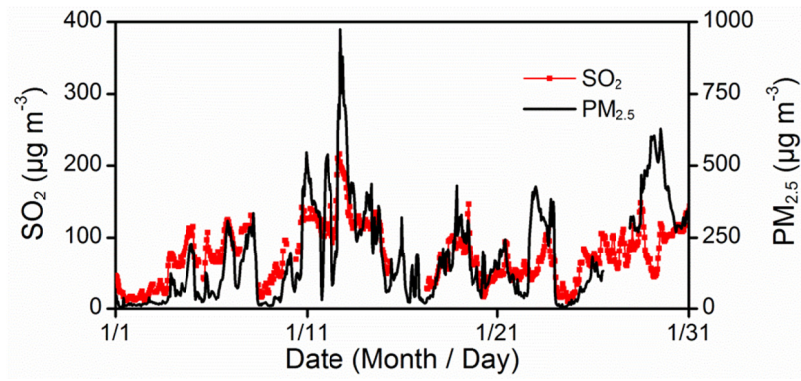
	CO ^a		NO ₂ ^a		SO ₂ ^a		PM _{2.5} ^a		PM ₁₀ ^a	
	Original	Revised	Original	Revised	Original	Revised	Original	Revised	Original	Revised
Data pairs	9338	9338	9366	9366	9384	9384	9335	9335	9143	9143
MeanObs	2.3	2.3	66.9	66.9	86.7	86.7	142.9	142.9	202.2	202.2
MeanSim	1.8	1.8	75.8	74.3	131.0	120.0	154.4	180.2	179.5	203.3
R	0.5	0.5	0.5	0.4	0.4	0.4	0.6	0.6	0.6	0.6
MB	-0.5	-0.5	9.0	7.5	44.4	33.4	11.5	37.3	-22.7	1.2
RMSE	1.5	1.5	35.3	34.1	119.1	110.5	86.9	111.0	116.1	122.5
NMB(%)	-20.6	-20.5	13.4	11.2	51.2	38.5	8.1	26.1	-11.2	0.6
NME(%)	43.3	43.3	41.9	39.4	91.6	84.6	41.3	54.3	38.1	42.4

1062 ^a The units of CO, NO₂, SO₂, PM_{2.5}, and PM₁₀ are mg m⁻³, μg m⁻³, μg m⁻³, μg m⁻³, and μg m⁻³,
 1063 respectively.

1064

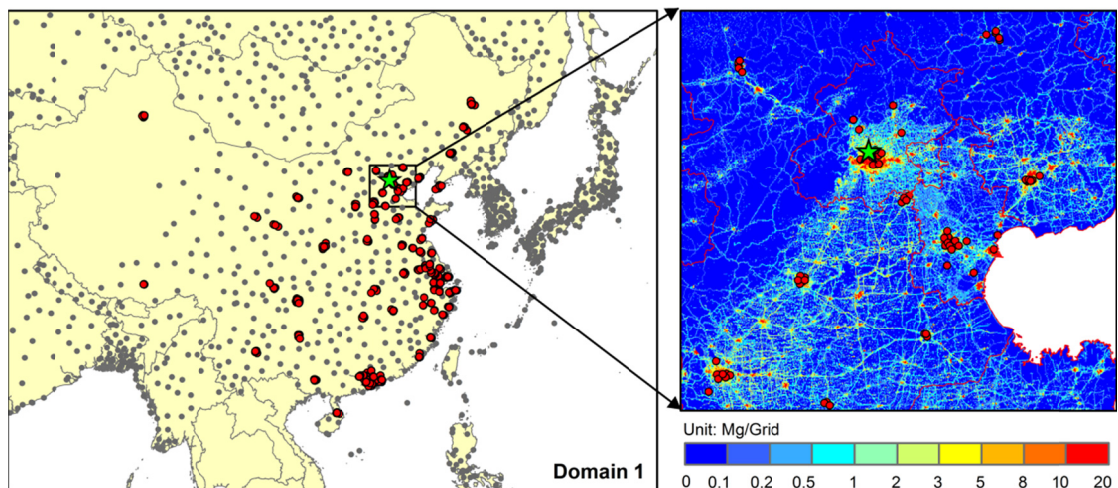
1065

1066



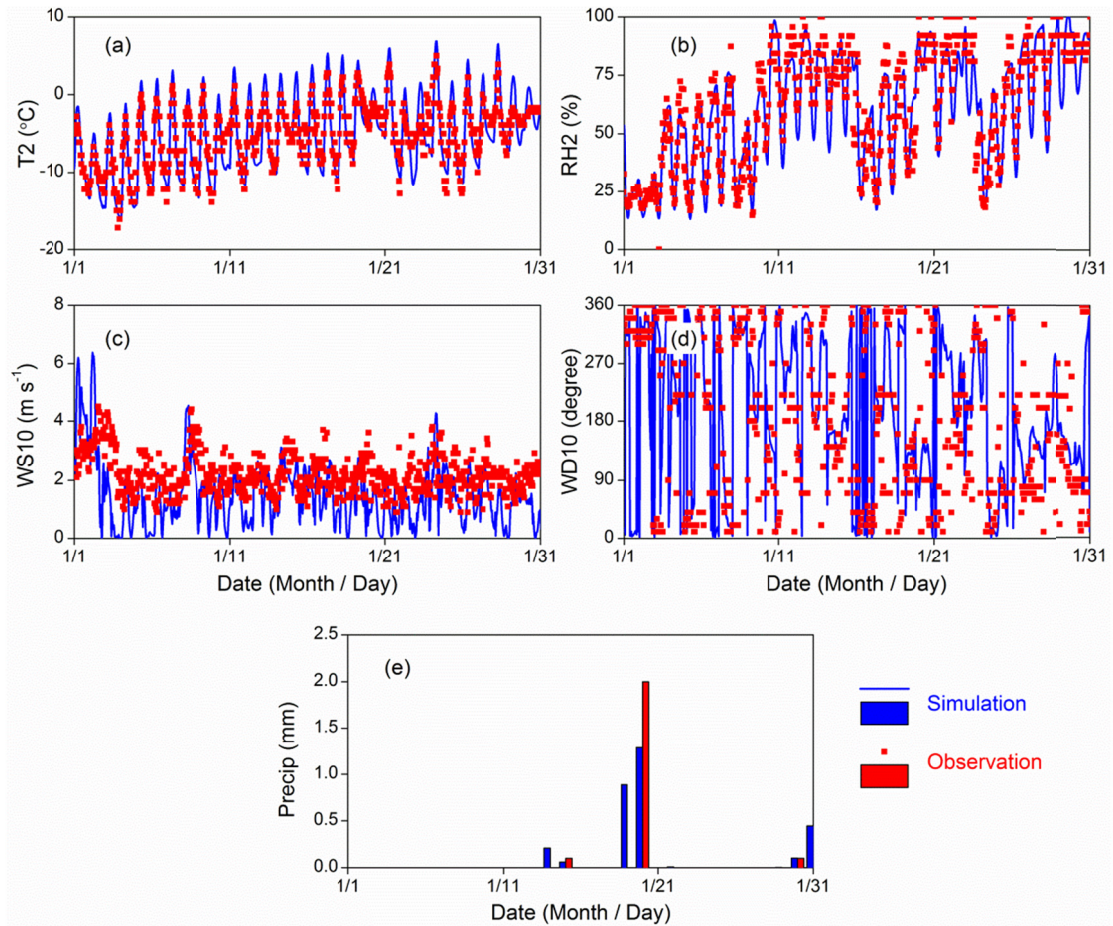
1068

1069 Figure 1. Observed concentrations of SO₂ and PM_{2.5} during January 2013 in Beijing.



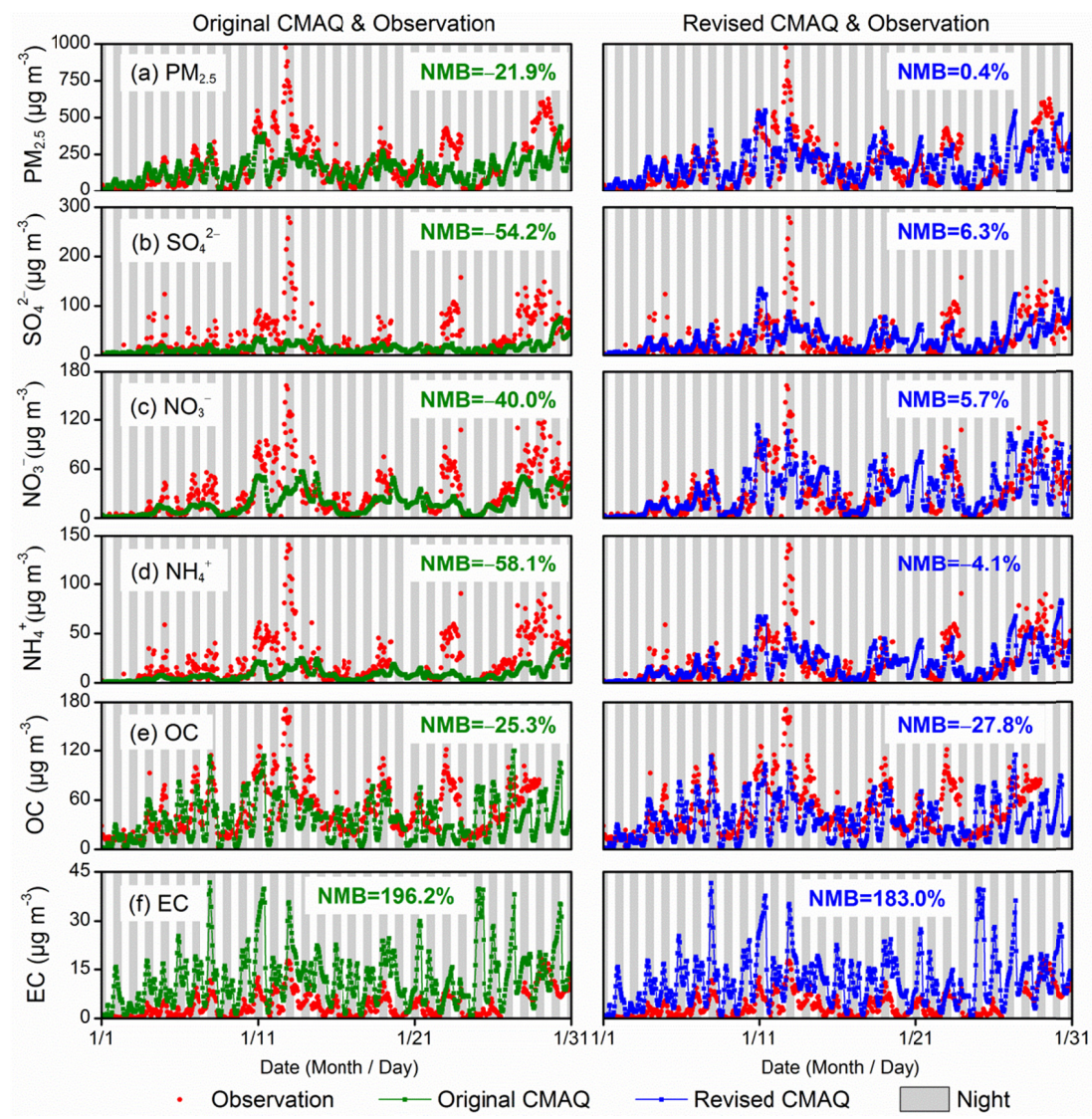
1070

1075 Figure 2. Simulation domain (Domain 1) and the monitoring stations. Gray circles are
 1076 meteorological stations included in the NCDC dataset and red circles are monitoring
 1077 stations included in the CNEMC dataset. Green star is the monitoring station at THU.
 1078 Background in the enlarged map is NO_x emission inventory of January 2013 at a
 1079 horizontal resolution of 1 km.



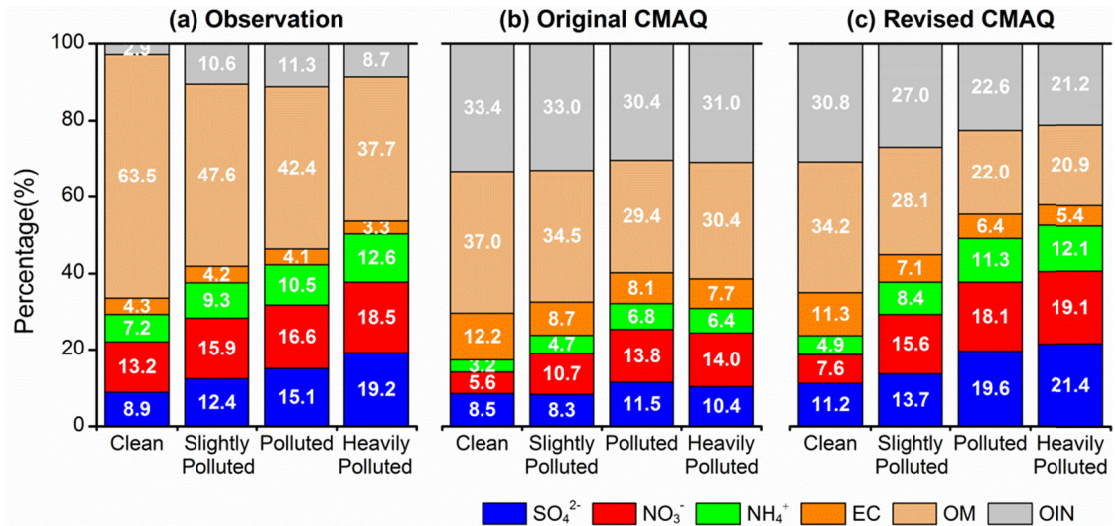
1076

1078 Figure 3. Observed and simulated meteorological variables at THU site: (a) hourly
 1079 T2; (b) hourly RH2; (c) hourly WS10; (d) hourly WD10; (e) daily Precip.



1079
 1082
 1083
 1084

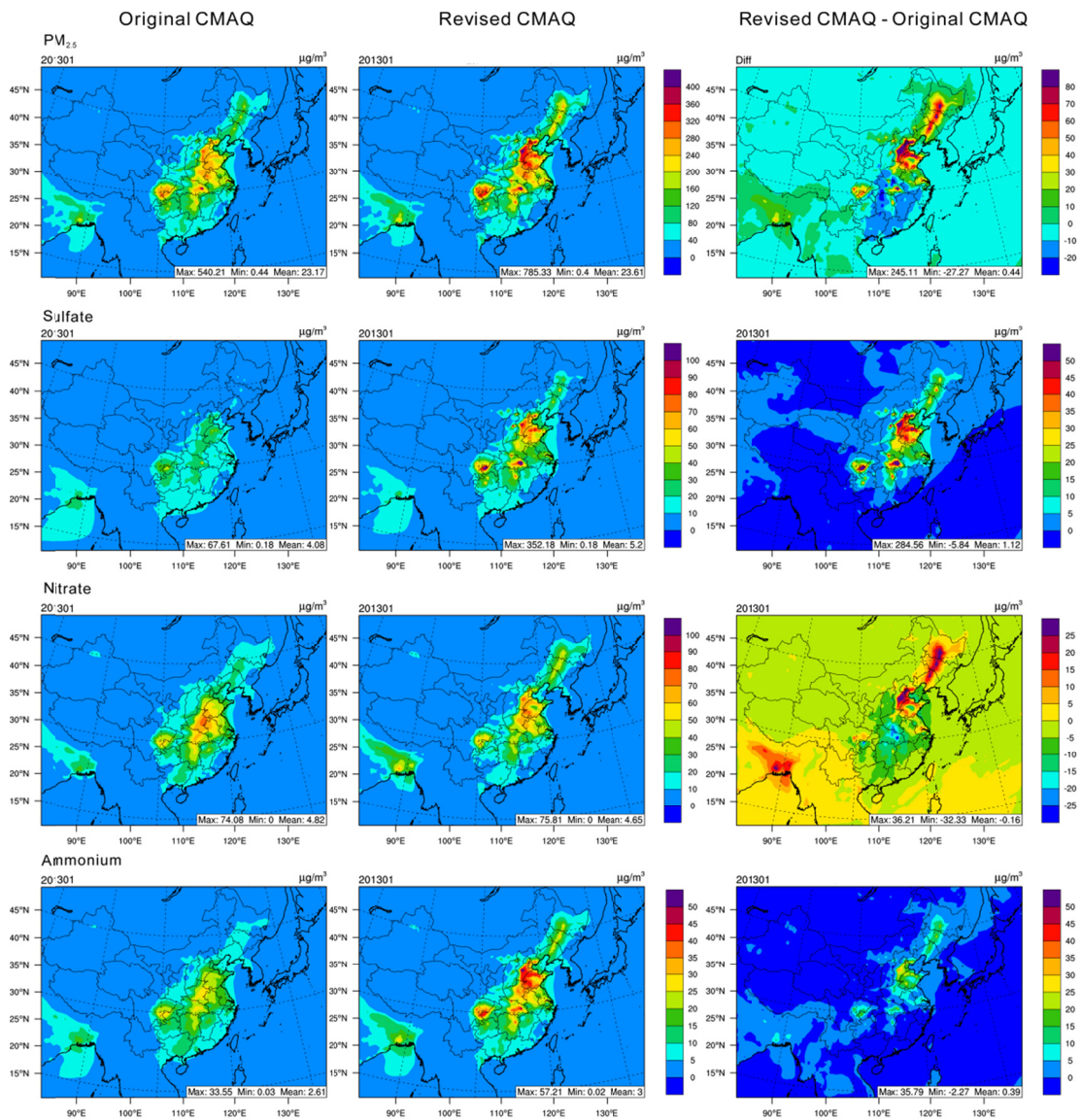
Figure 4. Observed and simulated hourly aerosol compositions from the original and revised CMAQ at the THU site: (a) $PM_{2.5}$; (b) SO_4^{2-} ; (c) NO_3^- ; (d) NH_4^+ ; (e) OC; (f) EC.



1083

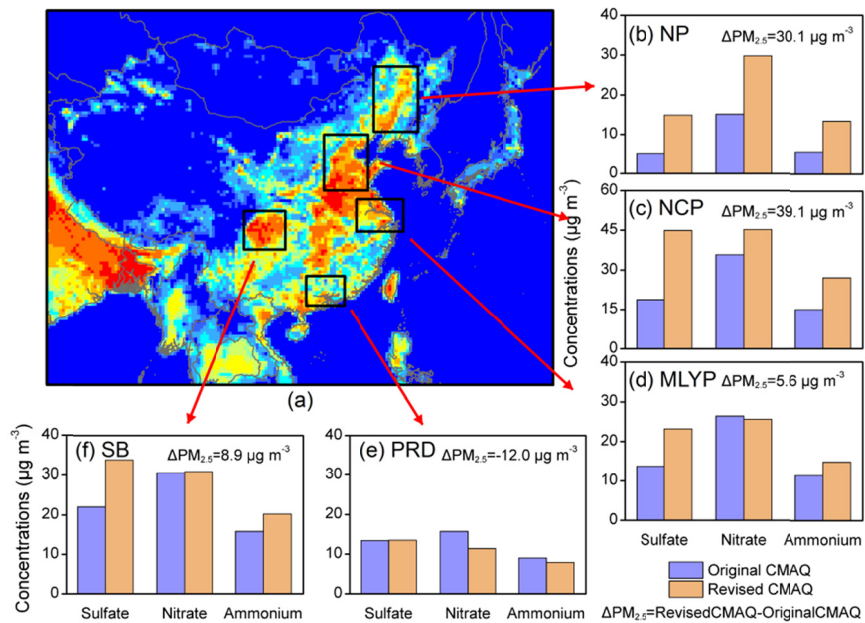
1091 Figure 5. Percentile compositions of major components in PM_{2.5} derived from (a)
 1092 Observation; (b) Original CMAQ; (c) Revised CMAQ with enhanced heterogeneous
 1093 chemistry. The pollution is classified into four types: clean (PM_{2.5} ≤ 35 μg m⁻³),
 1094 slightly polluted (35 < PM_{2.5} ≤ 115 μg m⁻³), polluted (115 < PM_{2.5} ≤ 350 μg m⁻³), and
 1095 heavily polluted (PM_{2.5} > 350 μg m⁻³), based on the China's Air Quality Index (AQI)
 1096 level definition.

1097 (<http://kjs.mep.gov.cn/hjbhbz/bzwb/dqhjbh/jcgfffbz/201203/W020120410332725219>
 1098 541.pdf)



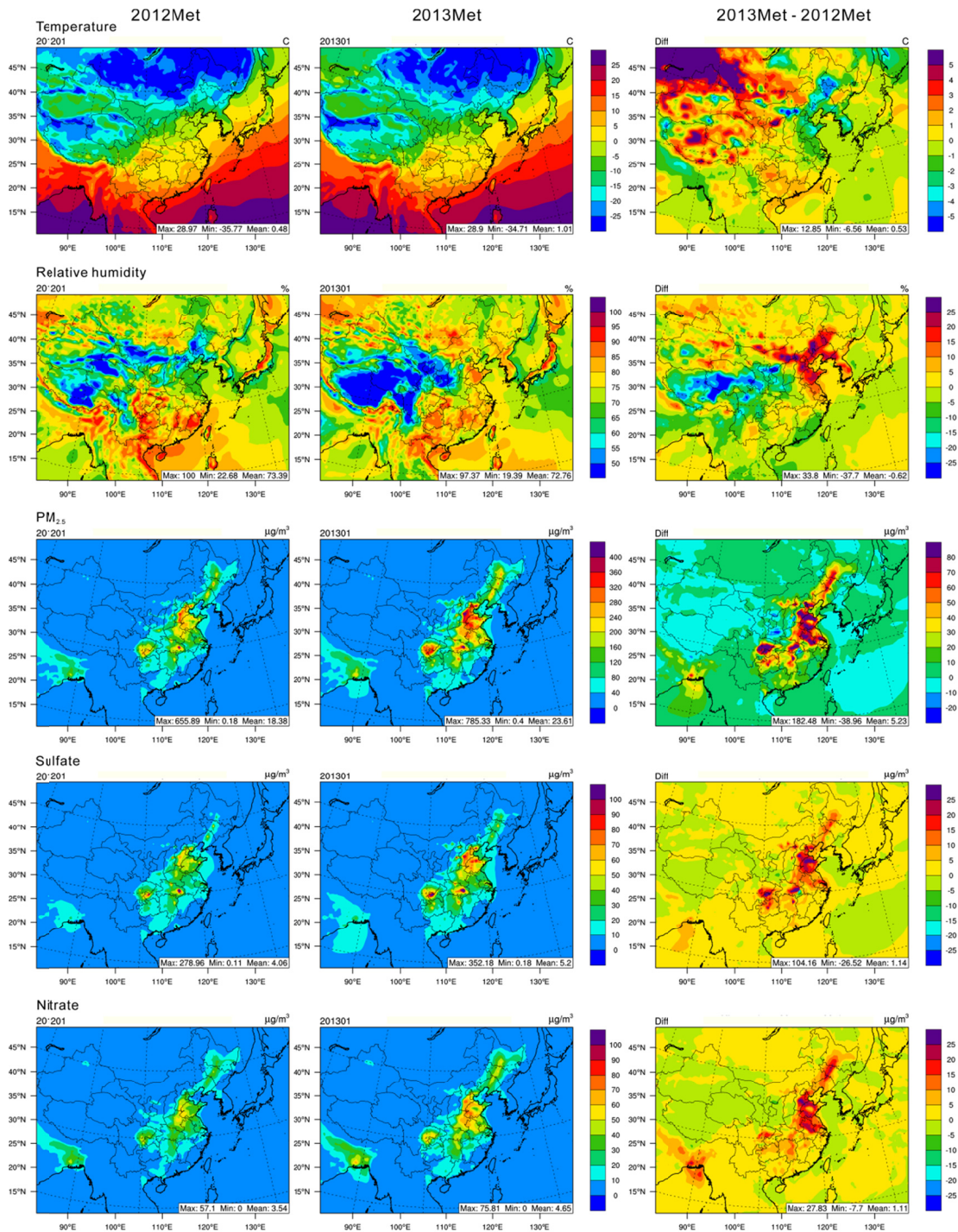
1092
 1096
 1097
 1098
 1099

Figure 6. Spatial distributions of monthly (January 2013) mean concentrations of PM_{2.5}, sulfate, nitrate, and ammonium simulated by the Original CMAQ (left), Revised CMAQ (middle), and the differences between the Revised and Original CMAQ (right).



1097

1100 Figure 7. Comparison of predicted SNA from Original and Revised CMAQ for (b)
 1101 NP, (c) NCP, (d) MLYP, (e) PRD and (f) SB. The figure (a) is the emission map of
 1102 NH_3 in January 2013 at a horizontal resolution of 36 km (source: MEIC model).



1101

1105

1106

1107

1108

1106

Figure 8. Spatial distributions of the monthly (January 2013) mean temperature, RH, and concentrations of $PM_{2.5}$, sulfate, and nitrate simulated by the revised CMAQ model with meteorological fields of 2012 (left) and 2013 (middle), and the differences between these two simulations (right).